Qubit based on spin-singlet Yu-Shiba-Rusinov states

Luka Pavešić and Rok Žitko*
Jožef Stefan Institute, Jamova 39, SI-1000 Ljubljana, Slovenia
and Faculty of Mathematics and Physics, University of Ljubljana, Jadranska 19, SI-1000 Ljubljana, Slovenia

(Received 2 December 2021; revised 7 February 2022; accepted 7 February 2022; published 15 February 2022)

The local magnetic moment of an interacting quantum dot occupied by a single electron can be screened by binding a Bogoliubov quasiparticle from a nearby superconductor. This gives rise to a long-lived discrete spin-singlet state inside the superconducting gap, known as the Yu-Shiba-Rusinov (YSR) state. We study the nature of the subgap states induced by a quantum dot embedded between two small superconducting islands. We show that this system has two spin-singlet subgap states with different spatial charge distributions. These states can be put in a linear superposition and coherently manipulated using electric-field pulses applied on the gate electrode. Such a YSR qubit could be implemented using present-day technology.

DOI: 10.1103/PhysRevB.105.075129

I. INTRODUCTION

The coupling of an impurity carrying a local magnetic moment to a superconductor (SC) produces discrete subgap states, known as Yu-Shiba-Rusinov (YSR) states [1–3]. These are spin-singlet bound states of Bogoliubov quasiparticles screening the impurity spin through antiferromagnetic Kondo exchange interactions. The energy gain from this coupling allows them to descend deep into the superconducting gap. Such subgap states appear in the spectra of many modern superconducting devices, where local magnetic moments arise in multiple ways, such as in adsorbed magnetic atoms or molecules, or in semiconductor quantum dots (QDs) [4–10].

Systems of this kind are commonly modeled by extending the Anderson impurity model [11] to the case of a superconducting bath, typically described by the BCS mean-field theory [12]. Such Hamiltonians can be reliably solved by various numerical approaches, with the numerical renormalization group (NRG) proving the most successful [13–18].

Recent developments of experimental techniques enabled the fabrication of epitaxial SC islands in hybrid semiconductor-SC devices that are small enough for the Coulomb repulsion between the electrons to be important [19,20]. This is taken into account by an effective charging term $E_C\hat{n}_{\mathrm{SC}}^2$, where $\hat{n}_{\mathrm{SC}}$ is the SC electron number operator and $E_C = e_0^2/2C$ is the charging energy with C the island's total capacitance [21–29]. Incorporating this term into existing numerical techniques proves very difficult for two reasons. First, the electron number is not a conserved quantity in the BCS theory, which makes the implementation of an electron number operator problematic [30]. Second, the Coloumbic repulsion of the SC electrons makes the bath an interacting system, resulting in a problem which cannot be solved by any traditional impurity solver. Most theoretical treatments were based on *ad hoc* pictures relying on physical intuition rather than solving microscopic models.

In a recent paper [31], we presented a numerical method which does not suffer from the described problems. We introduced a model that builds on previous work in the context of ultrasmall superconducting grains [23,32–34], where the Richardson-Gaudin charge conserving model of superconductivity [35–37] was successfully applied. This model describes the SC as a set of single-particle energy levels with an attractive all-to-all pairing interaction and is well suited for the description of small SC systems. Using such a model with a few hundred energy levels is very close to the BCS description appropriate in the thermodynamic limit but retains the advantage of a well-defined number of particles and thus the ability to include in a clean and well-defined manner the Coloumbic repulsion in the superconducting island into the model. Using the density matrix renormalization group (DMRG) [38–40] as the numerical solver, we are able to treat the charging term exactly and on the same level as other parameters and obtain accurate results in all parameter ranges. This approach was shown to give results in remarkable agreement with experiments in a setup of a QD with a single SC island [41]. The implementation based on matrix product states allows us to calculate basically any observable and allows for a detailed theoretical insight into the nature of the subgap states.

In this paper, we extend our analysis to a QD embedded between two SC islands. This is motivated by the considerable experimental interest in complex hybrid devices [42,43] and specifically in the two-channel problems where the impurity is coupled to two SCs, e.g., embedded in a Josephson junction [44–48]. In the absence of flux bias, to make the two SCs behave as two independent channels, at least one of them needs to have a significant charging energy. It may be noted that this is also a necessary condition for observing the two-channel Kondo effect in normal-state systems [25,49–52]. Coupling an impurity spin to two independent SC islands produces two singlet subgap states, as a Bogoliubov quasiparticle from either of the channels can screen the impurity spin [53]. In

*rok.zitko@ijs.si

this paper, we investigate the nature of these subgap states in realistic models of hybrid devices, focusing on the singlet symmetry sector with an even total number of electrons in the system.

This paper is organized as follows. In Sec. II, we introduce the model and discuss the technical issues arising from the presence of multiple superconducting regions. In Sec. III, we discuss the symmetric situation with two equivalent SCs, having the same SC gap Δ and the same charging energy E_C. In Sec. IV, we analyze the asymmetric situation with different charging energies (e.g., one large SC and one small superconducting island). In Sec. VI A, we model a realistic QD by reducing U, and thus moving away from the Kondo limit to an experimentally relevant regime. We briefly discuss the effect of decreased U and then proceed in Sec. VI with the gate tuning effects that ultimately reveal a regime propitious to operating such devices as a YSR qubit. In Sec. VII, we calculate the electric transition moments, quantities important for manipulation of subgap states. We close with a discussion and a conclusion.

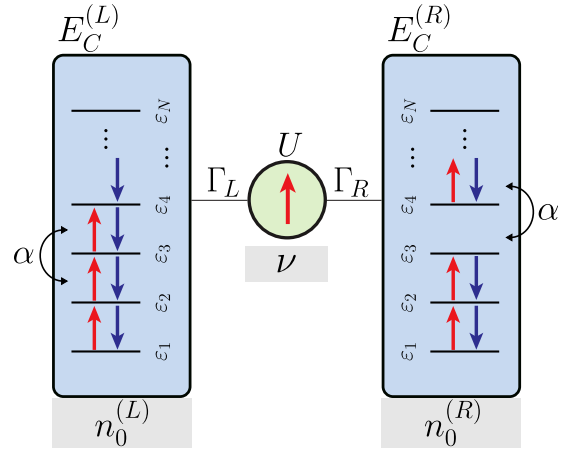

FIG. 1. Schematic representation of the system: An interacting quantum dot embedded between two superconducting islands with charging energies $E_C^{(L)}$ and $E_C^{(R)}$. The electron occupancy in the different parts of the device is tunable by the gate voltages $n_0^{(L)}$, $n_0^{(R)}$, and ν.

II. MODEL AND METHOD

A. Hamiltonian

The Hamiltonian consists of a single impurity level coupled to two SC islands [11,54,55]:

$$H = H_{\text{imp}} + \sum_{\beta=L,R} \left(H_{\text{SC}}^{(\beta)} + H_{\text{hyb}}^{(\beta)}\right), \tag{1}$$

where

$$H_{\text{imp}} = \varepsilon \hat{n}_{\text{imp}} + U \hat{n}_{\text{imp},\uparrow} \hat{n}_{\text{imp},\downarrow} = \frac{U}{2}(\hat{n}_{\text{imp}} - \nu)^2 + \text{const},$$

$$H_{\text{SC}}^{(\beta)} = \sum_{i,\sigma}^{N} \varepsilon_i c_{i,\sigma,\beta}^\dagger c_{i,\sigma,\beta} - \alpha d \sum_{i,j}^{N} c_{i,\uparrow,\beta}^\dagger c_{i,\downarrow,\beta}^\dagger c_{j,\downarrow,\beta} c_{j,\uparrow,\beta} + E_C^{(\beta)} \left(\hat{n}_{\text{SC}}^{(\beta)} - n_0^{(\beta)}\right)^2,$$

$$H_{\text{hyb}}^{(\beta)} = (v_\beta/\sqrt{N}) \sum_{i\sigma}^{N} (c_{i,\beta,\sigma}^\dagger d_\sigma + d_\sigma^\dagger c_{i,\beta,\sigma}).$$

Here ε is the energy level and U the electron-electron repulsion on the QD. The impurity term can be rewritten in terms of $\nu = 1/2 - \varepsilon/U$, the impurity level in units of electron number. d_σ and $c_{i,\beta,\sigma}$ are the annihilation operators corresponding to the QD and the two SC baths labeled by $\beta = L, R$ (left and right). The spin index is $\sigma = \uparrow, \downarrow$. Each SC bath is modeled by N energy levels ε_i spaced by a constant separation $d = 2D/N$, where $2D$ is the bandwidth. The levels are coupled all-to-all by a pairing interaction with strength α [54,55]. The SCs are coupled to the QD with the hybridization strengths $\Gamma_\beta = \pi \rho v_\beta^2$, where $\rho = 1/2D$ is the normal-state density of states in each bath. The number operators are $\hat{n}_{\text{imp}} = \sum_\sigma d_\sigma^\dagger d_\sigma$ for the impurity and $\hat{n}_{\text{SC}}^{(\beta)} = \sum_{i=1,\sigma}^{N} c_{i,\sigma,\beta}^\dagger c_{i,\sigma,\beta}$ for each SC bath. $E_C^{(\beta)}$ are the charging energies, with $n_0^{(\beta)}$ the optimal occupation of the SC island in units of electron charge. A sketch of the model system is shown in Fig. 1. In experimental setups, ν, $n_0^{(\beta)}$, and Γ_β are typically continuously tunable by the voltages applied to gate electrodes, while U, $E_C^{(\beta)}$, and Δ are device properties only weakly affected by the gate voltages.

If $E_C^{(L)} = E_C^{(R)}$, $n_0^{(L)} = n_0^{(R)}$, and $\Gamma_L = \Gamma_R$, the problem has a mirror (left-right) symmetry. In the absence of charging terms, the Hamiltonian then simplifies to a single-channel problem. This is easy to establish using an appropriate unitary transformation after a mean-field decoupling of the pairing terms. The same transformation applied to the original Hamiltonian leads to terms that mix states in both SCs (see Appendix A), but the effects of these terms become less physically significant with the increasing number of levels N, and disappear in the thermodynamic limit (with the gauge symmetry breaking).

B. Parameter choices

The calculations are performed for $N = 200$ energy levels in each SC. Using the half-bandwidth $D = 1$ as the energy unit, this corresponds to an interlevel spacing of $d = 2D/N = 0.01$. We choose $\alpha = 0.4$, which gives rise to the SC gap $\Delta = 0.165$ in each bath. This value is chosen so an appropriate number of levels is engaged in the pairing interaction, thus minimizing the finite-size effects while also minimizing the finite-bandwidth effect. Disregarding the finite-size corrections, the low-energy properties of the model are universally scalable by Δ.

We have implemented the Hamiltonian in the matrix product operator (MPO) form using matrices of dimension 9×9. The full expressions are given in Appendix B. We use the DMRG [38] to calculate the lowest eigenstates of the system in symmetry sectors defined by the total number of particles n and the total z component of spin S_z. We denote these by $|n, i\rangle$, with $i = 0$ the ground state (GS) in a given sector and $i = 1$ the first excited state (ES). The states with even n are spin singlets with $S_z = 0$, the states with odd n are spin doublets with $S_z = \pm 1/2$. The reference state $|\psi_{\text{ref}}\rangle$ is defined by filling the system with an even-integer number of electrons $\mathcal{N}$ in each SC and one electron in the QD for a total of

$n_{\rm ref} = 2\mathcal{N} + 1$ electrons. This spin-doublet state is the thermodynamic ground state of the system for $\nu = 1$, $n_0^{(\beta)} = \mathcal{N}$ in the limit $\Gamma_\beta \to 0$; it is a product state of two BCS wave functions in SCs (each projected to a fixed electron number $\mathcal{N}$) and a local moment on the QD site. We typically pick $n_{\rm ref}$ close to half filling $2N + 1$ to minimize the finite-size effects, but the results discussed in the following do not depend on this choice. The calculations are performed for states with total charge n spanning a narrow range around $n_{\rm ref}$.

The energies of the low-lying excitations and their nature are determined by the charge distribution controlled by $(n_0^{(L)}, \nu, n_0^{(R)})$ and the impurity couplings Γ_L, Γ_R. The parity of the occupation number in SC islands is important for superconducting pairing, resulting in the even-odd effect [56–61]. Even occupation is favored in each SC, while in the case of odd occupation a Bogoliubov quasiparticle is formed, increasing the energy by Δ. The charging energy E_C determines the energy cost of the situation where the filling of the superconducting island is different from n_0. If n_0 is an even integer, all excitations with odd SC island occupancy have a further energy cost of E_C. In SC islands, the charge gap therefore increases to $\Delta + E_C$. The picture is reversed if n_0 is tuned to an odd integer value. The energy of the even-occupancy SC GS is then increased by E_C, reducing the gap or even closing it completely at $E_C = \Delta$. Further increase of E_C then reopens the gap which gradually develops the character of a Coulomb blockade gap. By introducing the impurity coupling Γ, the unpaired Bogoliubov quasiparticles can antiferromagnetically bind to the impurity, giving rise to the YSR subgap states. The strength of the binding, and the resulting energy reduction, is characterized by Γ. The subgap spectrum of the single-channel model with charging energy was thoroughly investigated in Ref. [31].

C. Notation

The eigenstates of the full model can be qualitatively characterized through the results of a simplified calculation with a small number of energy levels (at a very rough level even for $N = 1$), which gives low-lying excitations that are in one-to-one correspondence with those of the full problem and smoothly converge to the correct result with increasing N. This motivates us to introduce a simplified notation for the basis states $|S_L, S_{\rm imp}, S_R\rangle$, where S_i denotes the spin in the left bath, at the impurity, and in the right bath, respectively. Thus the state consisting of an electron in the left bath bound into a spin-singlet state with the impurity electron is written as

$$|\phi_L\rangle = (|\downarrow, \uparrow, 0\rangle - |\uparrow, \downarrow, 0\rangle)/\sqrt{2}, \tag{2}$$

while the spin-singlet in the right bath is

$$|\phi_R\rangle = (|0, \uparrow, \downarrow\rangle - |0, \downarrow, \uparrow\rangle)/\sqrt{2}. \tag{3}$$

It must be stressed, however, that the excitations in the large-N limit are not single-particle states but rather collective many-body states involving many electron and hole states around the Fermi level.

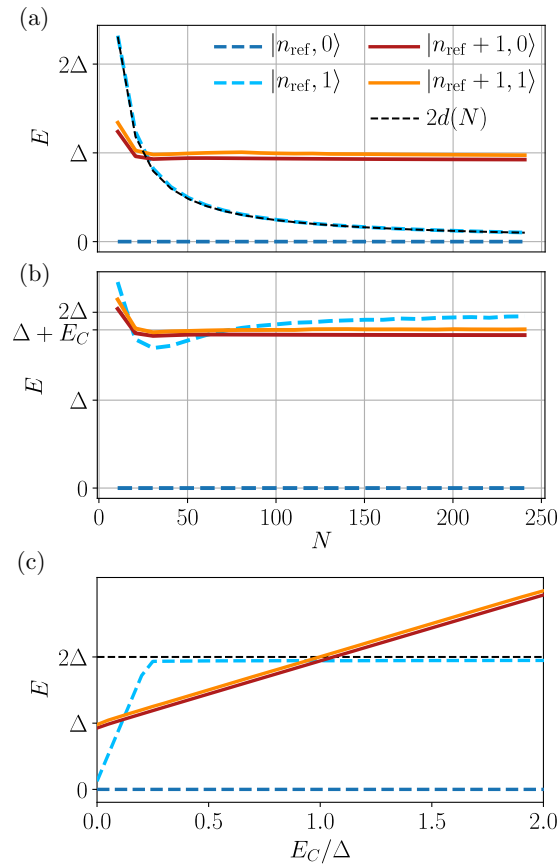

FIG. 2. (a), (b) System-size dependence of the subgap spectrum for small $\Gamma/U = 0.02$, when the subgap states barely detach from the continuum, for (a) $E_C = 0$ and (b) $E_C = 0.8\Delta$. (c) Subgap spectrum as a function of E_C at fixed system size $N = 200$. $U = 50\Delta$, $n_{\rm ref} = 2N + 1$ is an odd integer.

D. Fixed-phase versus fixed-charge superconducting states

In the BCS theory, the GS in the thermodynamic limit has broken symmetry. In the grandcanonical picture for a fixed phase of the SC order parameter, the GS does not have a well-defined number of particles: it is a superposition of states with $n, n + 2, n - 2, \ldots$ particles. Our model has, however, a finite size and we work in the microcanonical ensemble. The GS thus has a fixed number of particles, while the BCS phase is indeterminate. In calculations for a single SC bath, this poses no conceptual nor technical difficulty and the results are fully equivalent to those of the BCS theory in the limit of $N \to \infty$.

The situation is different in the presence of two SC baths with finite sizes. When they have small charging energies (the $E_C \to 0$ limit), one of them can act as a particle reservoir for the other. Let us consider the situation with $n_{\rm ref} = 2\mathcal{N} + 1$ electrons in the system for $\Gamma_i \to 0$. We find that the GS has $\mathcal{N}$ particles in each SC bath, the remaining one occupying the QD level. The first ES has a configuration $(\mathcal{N} + 2, \mathcal{N} - 2)$, i.e., one Cooper pair moves from one SC to the other at the energy cost of $2d$ and tending to zero in the thermodynamic limit, as shown in Fig. 2(a). It is important to stress that these (near) degenerate states are physical and not a numerical artifact. In the thermodynamic limit, the symmetry breaking

would fix the phase difference between the SC baths and eliminate all states save one by singling out the suitable linear superposition of (n_L, n_R) states. The lowest excitation in the equal-charge sector would then have energy 2Δ (i.e., the breaking of a single Cooper pair), as expected in the BCS picture. See Ref. [62], Chap. 7, for an in-depth discussion of physics in small superconducting grains.

In a finite-size system, the multitude of low-lying excitations for very small values of E_C poses a technical difficulty and, for example, hinders access to the more important Cooper-pair-breaking excitations on the scale of 2Δ. Due to the variational nature of DMRG, obtaining the ith ES requires the calculation of all i states with lower energy. While it is nominally possible to obtain many ESs, it is costly in time and computational resources, and the results are often not reliable, especially if the states are nearly degenerate, as is the case here. The same issue also arises in the spin-singlet sector, where each YSR singlet substrate would have replicas at slightly higher energies differing only in the distribution of the Cooper pairs between the SCs.

Fortunately, here we are interested in small systems which intrinsically have nonzero charging energies E_C. Moving a Cooper pair from one SC bath to another then costs $4E_C^{(L)} + 4E_C^{(R)}$. When this energy cost is larger than 2Δ, the $(\mathcal{N}+2, \mathcal{N}-2)$ states are pushed beyond the first excitation with the $(\mathcal{N}, \mathcal{N})$ configuration, which will then become the first ES of the system. We therefore constrain most of our calculation to the regime with $E_C^{(L)} + E_C^{(R)} > \Delta/2$, where there are no technical issues and the lowest-lying ES with a broken Cooper pair appears in the doublet sector, see Fig. 2(b), where $E_C^{(L)} = E_C^{(R)} = 0.8\Delta$. Figure 2(c) shows the evolution of the subgap spectrum with increasing E_C, illustrating the quick change in nature of the doublet ES when $E_C > \Delta/4$. As $\Gamma \approx 0$, the singlet $n_{\text{ref}} + 1$ states are barely below the quasicontinuum and therefore have energy marginally lower than $\Delta + E_C$.

We do not lose access to any important parts of the parameter space by the restriction to $E_C^{(L)} + E_C^{(R)} > \Delta/2$, as precise calculations in the thermodynamic limit are possible using the NRG for $E_C = 0$. Furthermore, for left-right mirror-symmetric problems, where the most relevant levels are the lowest ones in each parity subspace, the DMRG calculation could be implemented with the parity as a conserved quantum number after a suitable transformation of the Hamiltonian in the symmetry-adapted basis and an elaboration of its MPO form. Alternatively, one could target ESs with appropriate parity by adding weight terms that penalize states with undesired parity in the optimization sweeps. The required parity operator could be implemented using tensor index reordering.

III. SUBGAP STATES: CASE OF EQUIVALENT SUPERCONDUCTORS

In this section, we consider the simplest case of symmetric devices composed of two equivalent SCs, i.e., $E_C^{(L)} = E_C^{(R)} \equiv E_C$. We also set $n_0^{(L)} = n_0^{(R)} = \mathcal{N}$ with even integer $\mathcal{N}$ and restrict the discussion to the Kondo limit of $U/\Delta = 30$ and $\nu = 1$, where the occupation of the QD is pinned to 1.

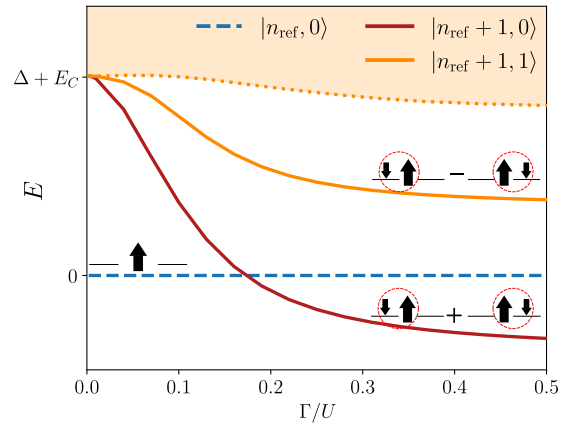

FIG. 3. Subgap spectrum for $\Gamma_L = \Gamma_R \equiv \Gamma$ and equal charging energies $E_C^{(L)} = E_C^{(R)} = 0.4\Delta$. At each Γ, the energy of the lowest doublet state is taken as the reference value for energies, i.e., $E(n = n_{\text{ref}}, i = 0) \equiv 0$. The subgap states are accompanied by sketches indicating their nature: the large spin represents the impurity electron, the small arrows denote the Bogoliubov quasiparticles, and the red circles represent a singlet configuration of the encircled levels, $|{\uparrow\downarrow}\rangle - |{\downarrow\uparrow}\rangle$. The orange shaded area above the orange dotted line denotes the quasi continuum of states in the $n_{\text{ref}} + 1$ sector.

A. Symmetric QD coupling

We first examine the case of symmetric coupling of the impurity to both baths, $\Gamma_L = \Gamma_R \equiv \Gamma$. The system then has mirror symmetry and we denote the corresponding parity as gerade/ungerade in the following. The low-lying states with an odd number of electrons n_{ref} (spin doublets) and an even number $n_{\text{ref}} + 1$ (spin-singlets) are shown in the form of an energy-level diagram in Fig. 3. For $\Gamma = 0$, the GS is a product state consisting of a BCS-like state of Cooper pairs in each channel and a decoupled electron sitting at the impurity site. The lowest ES with $n_{\text{ref}} + 1$ electrons is the Bogoliubov state at the bottom of the quasicontinuum (represented using orange shading) with energy $\Delta + E_C$; the presence of the quasicontinuum of Bogoliubov states is confirmed by calculating a number of higher ESs.

For $\Gamma > 0$, two states detach from the continuum to become the spin-singlet subgap states. This is clearly different from the situation in the $E_C = 0$ limit, where only the gerade state is inside the gap, while the ungerade combination is fully decoupled from the impurity and remains inside the continuum (in the absence of flux bias [8,63]; see Appendix A). With increasing Γ, both states descend deeper into the gap, with the gerade state always having lower energy. This is different from the situation in the two-channel Kondo model where the two subgap states are degenerate for equal exchange coupling constants [53]. This disparity is due to the interchannel charge fluctuations included in our (realistic) model, which materialize as off-diagonal terms in the effective exchange coupling matrix $J_{\alpha\beta}$ obtained with the Schrieffer-Wolff transformation [64]. These separate the gerade and ungerade eigenstates in energy, and correspond to different YSR wave functions, with an antinode and a node at the impurity site for the gerade and ungerade combinations of Bogoliubov states, respectively. In short, a two-channel Kondo model with symmetric exchange

coupling does not correspond to a two-channel single impurity Anderson model with symmetric hybridization terms.

The continuum of excitations in the $n_{\rm ref}+1$ sector begins at $\Delta+E_C$. At $\Gamma=0$, it consists of product states of the BCS-like state with $n_{\rm ref}$ electrons and a Bogoliubov quasiparticle in one of the channels. The lowest lying continuum states are $|\psi_{\rm ref}\rangle\otimes({\rm QP}_L\pm{\rm QP}_R)/\sqrt{2}$, where ${\rm QP}_\beta$ denotes a Bogoliubov quasiparticle in channel β. The small deviation from the $\Gamma=0$ gap value of $\Delta+E_C$ is due to the $\propto\Gamma^2$ virtual tunneling of quasiparticles between the channels; these processes are suppressed if E_C and/or U are increased.

The nature of the subgap singlets is investigated in Fig. 4. The first subgap state is an even (gerade) linear combination of spin-singlet YSR states from each channel.

$$\begin{aligned}|n_{\rm ref}+1,0\rangle &= |\psi_g\rangle\approx(|\phi_L\rangle+|\phi_R\rangle)/\sqrt{2}\\ &= \tfrac{1}{2}[(|\downarrow,\uparrow,0\rangle-|\uparrow,\downarrow,0\rangle)+(|0,\uparrow,\downarrow\rangle\\ &\quad-|0,\downarrow,\uparrow\rangle)]\\ &= \tfrac{1}{2}[(|\downarrow,\uparrow,0\rangle+|0,\uparrow,\downarrow\rangle)-(|\uparrow,\downarrow,0\rangle\\ &\quad+|0,\downarrow,\uparrow\rangle)],\end{aligned}\tag{4}$$

where the final line shows that this state may also be interpreted as a spin-singlet formed between the impurity spin and an even-parity combination of Bogoliubov excitations from both electrodes, while the second is an odd (ungerade) combination of the singlets,

$$\begin{aligned}|n_{\rm ref}+1,1\rangle &= |\psi_u\rangle\approx(|\phi_L\rangle-|\phi_R\rangle)/\sqrt{2}\\ &= \tfrac{1}{2}[(|\downarrow,\uparrow,0\rangle-|\uparrow,\downarrow,0\rangle)-(|0,\uparrow,\downarrow\rangle\\ &\quad-|0,\downarrow,\uparrow\rangle)]\\ &= \tfrac{1}{2}[(|\downarrow,\uparrow,0\rangle-|0,\uparrow,\downarrow\rangle)-(|\uparrow,\downarrow,0\rangle\\ &\quad-|0,\downarrow,\uparrow\rangle)],\end{aligned}\tag{5}$$

with an alternative interpretation as a spin-singlet formed between the impurity spin and an odd-parity combination of Bogoliubov electrons from both electrodes. The parity of the states is confirmed by the calculation of the one-particle density matrices in the baths, $\rho_{ij}=\langle c_i^\dagger c_j\rangle$, at finite Γ, shown in Fig. 4(a). The intrachannel correlations are in large part the result of superconducting pairing: ρ_{ij} is large for the levels which contribute to the creation of Cooper pairs and small between levels that are fully occupied or empty. The interchannel correlations uncover the nature of the states. Positive ρ_{ij} in the center of the interchannel correlation (off-diagonal blocks) in the left panel is a characteristic feature of a gerade configuration, while the negative values (right panel) are a feature of an ungerade state.

In Fig. 4(b), we illustrate the different composition of the two YSR singlets despite $\Gamma_L=\Gamma_R$, thus further revealing the differences compared to the pure two-channel Kondo model. We plot excess charge compared to a reference doublet state (left) and the spin-spin correlations $\langle\mathbf{S}_{\rm imp}\cdot\mathbf{S}_i\rangle$ between the impurity local moment and the SC single-particle energy levels $i=1,\ldots,N$, with energies between -1 and 1 (right). Both plots indicate that the singlet is formed between the impurity and the excess electron, which is located close to the Fermi level, but the charge distribution is not identical in the two

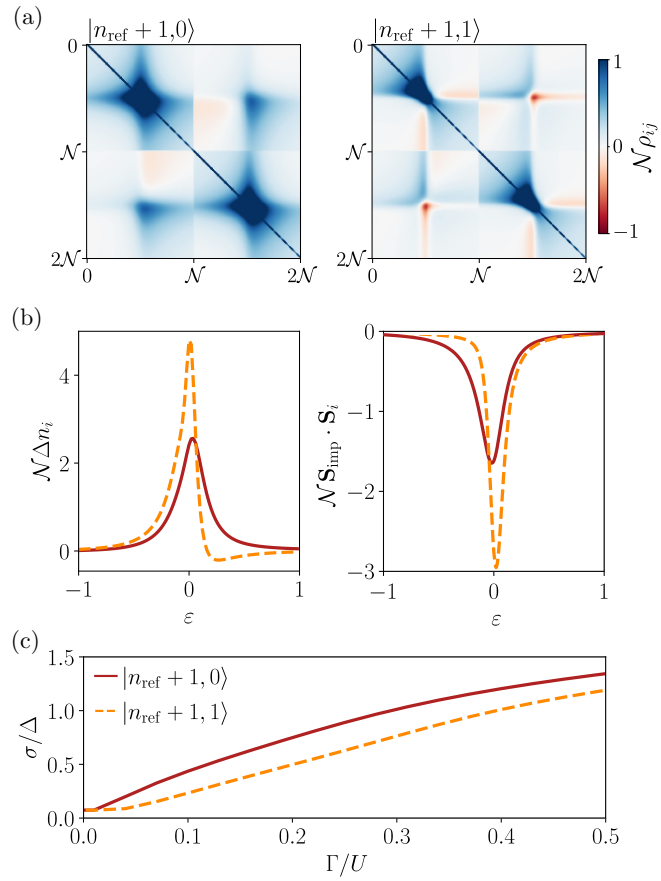

FIG. 4. Singlet subgap states. (a) Channel density matrix $\rho_{ij}=\langle c_i^\dagger c_j\rangle$ for the two singlet subgap states. $\Gamma/U=0.2$, $E_C=0.4\Delta$. The diagonal blocks represent intrachannel density matrices, while the off-diagonal parts represent the interchannel correlations. (b) Occupation and spin-spin correlations between the impurity and the baths. Δn_i is the excess charge compared to the reference doublet state at $\Gamma\to0$. $\Gamma/U=0.2$, $E_C=0.4\Delta$. (c) Γ dependence of the width of the spin-spin correlation peak. $E_C=0.4\Delta$.

states. The width of the spin-spin correlation peak with increasing Γ is shown in Fig. 4(c) and is in qualitative agreement with the well-known Kondo limits. At large coupling, the impurity is screened by the electron localized at $r=0$, with a broad distribution in energy, while at small coupling the screening is performed by the electrons with energies close to Fermi energy.

B. Asymmetric QD coupling

We now examine the case of $\Gamma_L\neq\Gamma_R$, see Fig. 5. We fix $\Gamma_L+\Gamma_R=0.1U$ and study the effect of the deviation from the equal-Γ tuning by simultaneously increasing Γ_R and decreasing Γ_L. The energy diagram in Fig. 5(a) is accompanied by Figs. 5(b) and 5(c), illustrating the nature of the singlet states. In Fig. 5(b), the deviation from half-filling (even integer $\mathcal{N}=(n_{\rm ref}-1)/2$) in each SC island is plotted. As we are in the limit of a very large U/Δ, the impurity occupation always remains very close to 1. Therefore, this plot uncovers the position of the unpaired quasiparticle in the SC channels. The impurity-channel spin-spin correlations, defined by

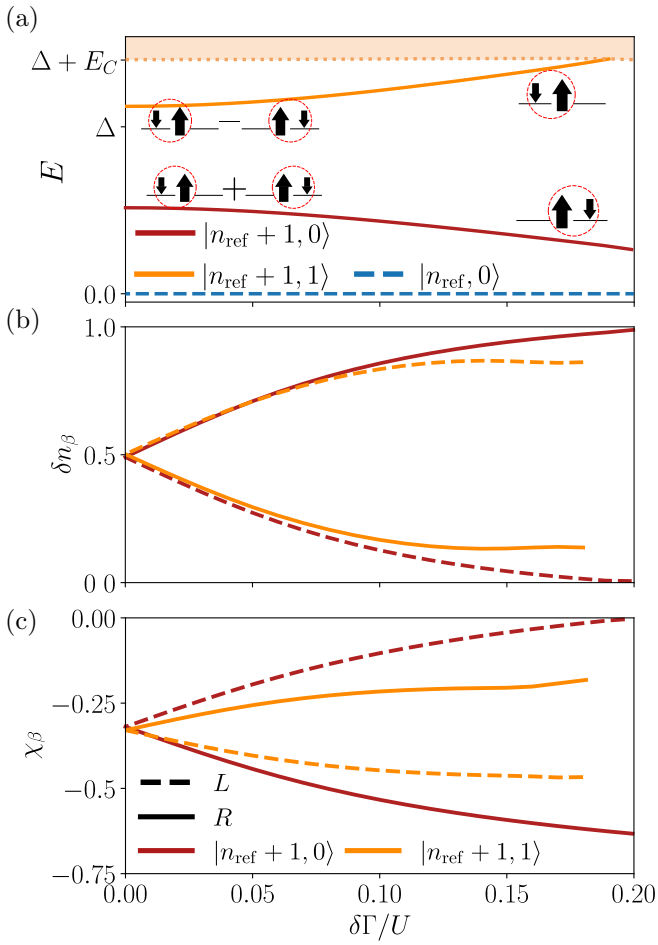

FIG. 5. Equivalent superconductors, asymmetric QD coupling. The dependence of the subgap states on $\delta\Gamma = \Gamma_R - \Gamma_L$ with the sum $\Gamma_L + \Gamma_R = 0.2U$ kept constant. (a) Subgap spectrum. Subgap states are accompanied by sketches indicating their nature. The orange shaded area represents the continuum of states in the $n_{\rm ref}+1$ sector. (b) Deviation from half filling in the superconductors for the singlet subgap states. (c) Spin-spin correlations between the impurity and the baths for the singlet subgap states. The value of $-3/4$ corresponds to a pure (saturated) singlet configuration.

$\chi_\beta = \sum_{i=1}^{N}\langle \mathbf{S}_{\rm imp}\cdot\mathbf{S}_i^{(\beta)}\rangle$ are presented in Fig. 5(c) and contain information on the screening of the impurity local moment.

With increasing $\delta\Gamma$, the nature of the subgap states gradually changes from the inversion-symmetry eigenstates $|\psi_g\rangle$ and $|\psi_u\rangle$ with equal χ in both channels to states that are closer to simple YSR singlets $|\phi_L\rangle$ and $|\phi_R\rangle$. The state with the lowest energy is the one corresponding to the larger hybridization (Γ_R in our case, so $|\phi_R\rangle$), while the excited subgap state transforms into $|\phi_L\rangle$. The energy of the excited subgap state increases as Γ_L is decreased, and it finally merges with the continuum when the left channel decouples from the system at $\delta\Gamma \to 0.2$ (therefore, $\Gamma_L \to 0$). This is different from the superconducting two-channel Kondo model, where breaking the coupling symmetry quickly pushes the second ES beyond the gap [53]. We note also that in the normal-state two-channel Kondo problem, a small difference in couplings immediately leads to a crossover to a Fermi-liquid fixed point

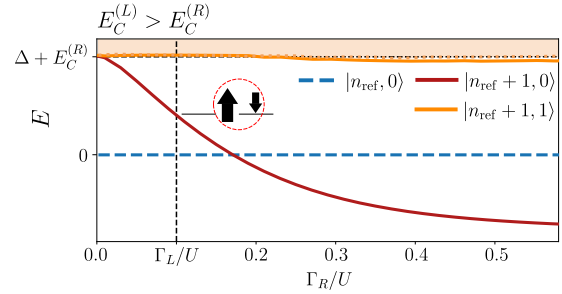

FIG. 6. Nonequivalent superconductors, $E_C^{(L)} \gg E_C^{(R)}$. Subgap spectra dependence on Γ_R for constant Γ_L/U with $E_C^{(L)} = 0.1\Delta$, $E_C^{(R)} = 1.5\Delta$. The value of Γ_L/U is indicated by the vertical dashed line.

strictly at zero temperature, with one of the channels completely decoupled. In problems with a superconducting gap, the renormalization is terminated at the scale of the gap, thus a complete decoupling of a second channel does not occur except in the cases of extreme asymmetry.

IV. SUBGAP STATES: CASE OF NONEQUIVALENT SUPERCONDUCTORS

The experimental interest in devices where the QD is embedded between one macroscopic SC contact and one SC island provides the motivation for considering the case of strongly differing charging energies. The asymmetry in the charging energies induces a preference for optimal occupation in the channel with larger E_C, which is even for $n_0^{(\beta)}$ tuned to an even value. In the singlet sector with an even total number of particles, this implicitly favors the spin-singlet YSR state formed between the impurity spin with a decoupled Bogoliubov quasiparticle in the channel with smaller E_C.

In this section, the results will be presented by plotting the evolution of the subgap states with changing Γ_R at fixed Γ_L for several different cases of nonequivalent SC parameters.

A. General considerations

Unequal charging energies influence the subgap states in one important aspect. The transition from the ungerade/gerade regime at small $\delta\Gamma$ toward $|\phi_L\rangle/|\phi_R\rangle$ subgap states at large $\delta\Gamma$ is decelerated (i.e., requires larger $\delta\Gamma$) if the strongly coupled channel has larger charging energy. The hybridization favors configurations with the unpaired particle in the strongly coupled channel, while its charging energy enforces even occupation. The crossover occurs only when the larger Γ is big enough to overcome the charging-energy penalty. This is demonstrated in Appendix C using a zero-bandwidth calculation.

B. Case of $E_C^{(L)} \gg E_C^{(R)}$

If the difference in E_C is very large, this mechanism may cause the weakly coupled channel with large charging energy to almost completely decouple from the system. Such decoupling is illustrated in Fig. 6 for the case of $E_C^{(L)} \gg E_C^{(R)}$. The second subgap state does not descend deeper into the gap even for very large Γ_R, and we effectively obtain a single

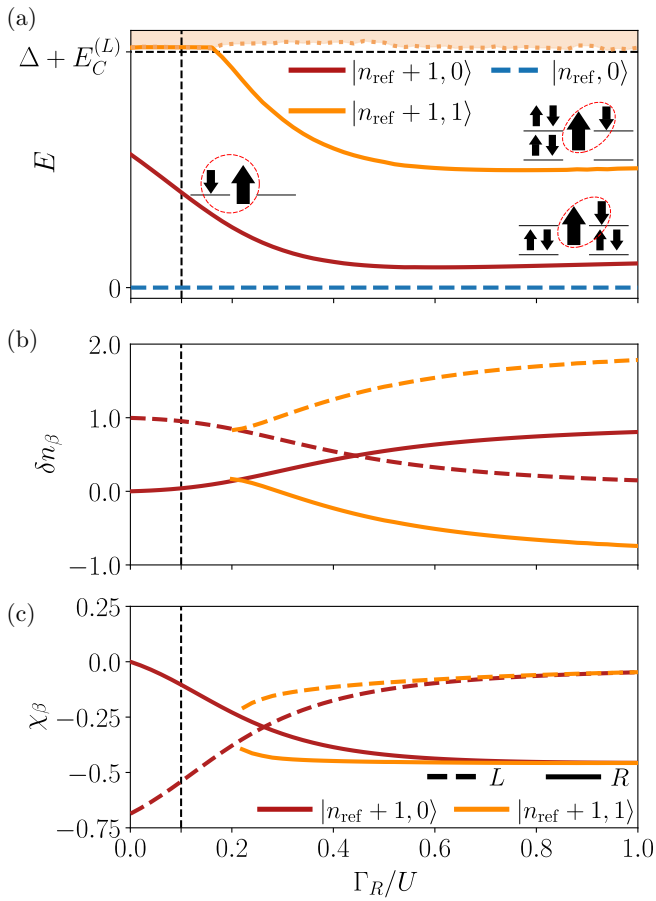

FIG. 7. Nonequivalent superconductors, $E_C^{(L)} \ll E_C^{(R)}$. (a) Subgap spectrum dependence on Γ_R for constant $\Gamma_L/U = 0.1$ ($\Gamma_L = \Gamma_R$ tuning is indicated by the vertical dashed line). The states are accompanied by sketches of the charge configurations. The blue ovals represent Cooper pairs. (b) Deviation from half filling in the superconducting islands of the singlet subgap states. (c) The impurity-channel spin-spin correlation of the singlet subgap states. $E_C^{(L)} = 0.1\Delta$, $E_C^{(R)} = 1.5\Delta$.

channel YSR singlet in the right channel, with a barely visible contribution from the left one.

C. Case of $E_C^{(L)} \ll E_C^{(R)}$

The subgap spectrum is most intriguing in the regime of $E_C^{(L)} \ll E_C^{(R)}$. The charging terms favor even occupation in the right channel, therefore singlet screening in the left. For low $\Gamma_R < \Gamma_L$, we observe the decoupled situation with a single subgap singlet $|\phi_L\rangle$ and a decoupled right channel, Fig. 7. When Γ_R increases beyond Γ_L, the system transitions into the regime where the hybridization terms favor $|\phi_R\rangle$, which is at the same time strongly disfavored by the charging energies. The lower subgap state transforms into a right-channel singlet state only for $\Gamma_R \gg \Gamma_L$, when the strong hybridization eventually overcomes the energy penalty due to $E_C^{(R)}$. The excess charge and impurity-channel spin correlations shown in Figs. 7(b) and 7(c) illustrate the smooth transition of the lower singlet state between the $|\phi_L\rangle$ and $|\phi_R\rangle$ limits. The spin correlations do not reach the saturated singlet value of $-3/4$,

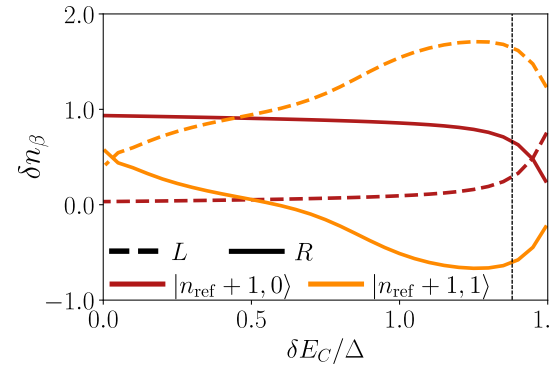

FIG. 8. Evolution of the deviation from half filling in the superconducting islands with varying charging energy asymmetry. The sum $E_C^{(L)} + E_C^{(R)} = 1.5\Delta$ is kept constant, with $\delta E_C = E_C^{(R)} - E_C^{(L)}$. $\Gamma_L = 0.1U$, $\Gamma_R = U$. The vertical dashed line roughly corresponds to the rightmost point of Fig. 7(b).

indicating that even for very large Γ_R this state never quite obtains the nature of a pure singlet.

A second subgap state descends into the gap at some finite Γ_R. Curiously, this $i = 1$ subgap state is not a left-channel YSR singlet as one might expect. Instead, the spin correlations show a very close relation to the $i = 0$ subgap state, increasingly so as Γ_R grows large. It transpires that the $i = 1$ is obtained from the $i = 0$ state by a transfer of a Cooper pair between the SCs, i.e., while the $i = 0$ state has charge configuration $(\mathcal{N}, 1, \mathcal{N}+1)$, the $i = 1$ state corresponds to $(\mathcal{N}+2, 1, \mathcal{N}-1)$. This allows the ES to also obtain the energetically optimal nature of a right-channel YSR singlet. The transfer of two additional electrons only costs $4E_C^{(L)}$, corresponding to approximately 0.4Δ in the example shown (plus $2d$, a finite size effect).

The evolution of the channel occupation with increasing E_C asymmetry is shown in Fig. 8. By increasing δE_C (decreasing $E_C^{(L)}$ and increasing $E_C^{(R)}$), the second subgap state approaches the $(\mathcal{N}+2, 1, \mathcal{N}-1)$ limit. For the parameters chosen here, the charging energy penalty overcomes the Γ coupling just as $E_C^{(L)} \to 0$ and the occupation of the subgap states tends toward even occupation in the right channel, following the dominant charging energy effect. It should be stressed that the existence of such an ES is not a numerical artifact but rather a signature of the physics of small SC islands with large charging energies.

D. YSR spin-singlet qubit

The regime of $E_C^{(L)} < E_C^{(R)}$ with $\Gamma_L < \Gamma_R$ seems to be the most appropriate for the investigation of the occurrence of two singlet subgap states, both well separated from the quasicontinuum at higher energies. In particular, it appears possible to achieve energy separation between the singlets that is lower than the transition energy from the upper level to the continuum. This is required for the implementation of qubits based on a linear superposition of the YSR singlet states, a *YSR qubit*. The relative position of the states is highly tunable: the energy difference from the gap edge is increased by increasing Γ_R. The energy difference between states depends on $E_C^{(L)}$, which is typically a device property. If $E_C^{(L)}$ is

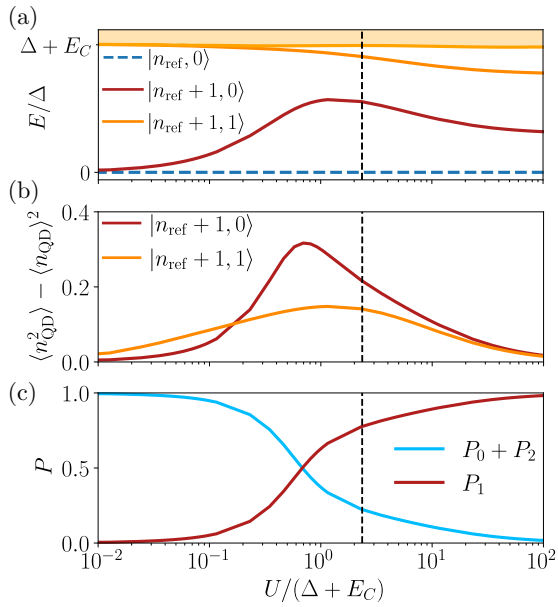

FIG. 9. U dependence of the subgap states. (a) Subgap spectrum as a function of U. (b) QD charge fluctuations in the subgap singlet states. (c) Probabilities P_n that in the lowest singlet state the QD is occupied by n electrons. Here we show the symmetric case with constant $\Gamma = \Gamma_L = \Gamma_R = 0.1U$, $E_C = E_C^{(L)} = E_C^{(R)} = 0.7\Delta$. U is scaled by $\Delta + E_C$, the first being the charging energy scale of the QD and the latter of the SC islands. The vertical line at $U/\Delta = 4$ corresponds to the regime in which realistic devices operate.

small, there will be further singlet states with two, three, etc. Cooper pairs transferred between the SCs, but the energy cost for those increase quadratically, resulting in nonmonotonic spacing.

We further investigate this parameter regime in Sec. VI by considering the effects of tuning of the gate voltages in the system. These determine the favorable occupation of the system components, which can strongly influence the nature of the subgap states.

V. REALISTIC QD

While the Kondo limit of large electron-electron repulsion on the QD, $U \gg \Delta$, is useful for studying the nature of the YSR subgap states in an ideal setting, a large class of real devices in current use operate in the regime of comparable parameter values, $U \approx \Delta \approx E_C$. By decreasing U, we move away from the Kondo limit where the QD behaves almost as a pure magnetic impurity, thus changing the nature of the subgap states from the YSR singlets (due to Kondo exchange interaction) by increasing the admixture of wave functions with Andreev bound state (ABS) character (due to proximity effect) and the role of Coulomb interaction. The changing nature of the subgap singlets as a function of U is demonstrated in Fig. 9. We consider a symmetric case with constant $\Gamma/U = 0.1$ and $E_C = 0.7\Delta$. The level diagram in Fig. 9(a) shows that the energy difference between the subgap singlets is constant at large U/Δ, determined mostly by Γ/U. With decreasing U, the upper singlet disappears into the continuum, while the lower one approaches the energy of the doublet GS.

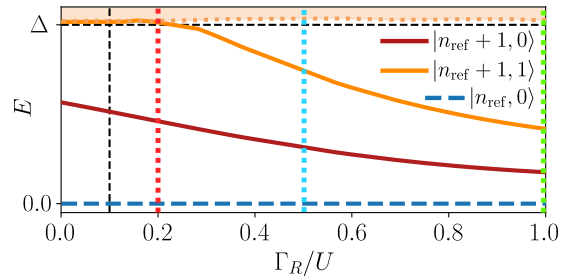

FIG. 10. Realistic $U = 4\Delta$ and $E_C^{(L)} \ll E_C^{(R)}$. Subgap spectra dependence on Γ_R at constant $\Gamma_L/U = 0.1$, indicated by the black vertical dashed line. $E_C^{(L)} = 0.1\Delta$, $E_C^{(R)} = 1.5\Delta$. The vertical dotted lines correspond to $n_0^{(R)}$ sweeps presented in Fig. 11.

In the absence of charging energy, a pair of singlet ABS states is expected, with energy symmetrically above and below the doublet state, the difference between them determined by Γ. As Γ/U is constant in our plot, $U \to 0$ means $\Gamma \to 0$ as well. This is why the lowest singlet and doublet states appear degenerate in the limit of small U. Furthermore, the charging energy breaks the degeneracy between the states with a different number of Cooper pairs in the SC islands, thus creating an energy difference between the $|0\rangle$ and $|2\rangle$ states on the QD. The impurity in the ground single state has predominantly double occupancy, while in the ES it is predominantly empty. The energy cost of the ES is $4E_C$ (for an additional Cooper pair in the SC), so this state lives far beyond the continuum of decoupled excitations. The QD charge fluctuations are presented in Fig. 9(b). They are small in the Kondo limit at $U \gg \Delta$, where the QD is a pure magnetic impurity and the only charge fluctuations correspond to virtual processes that generate the Kondo exchange scattering $J_K \propto \Gamma/U$. The charge fluctuations are also small for $U \ll \Delta + E_C$, because the charging effects in the SC islands strongly determine the QD occupation. They are hence the strongest in the crossover regime, which is where the experimental devices operate. Finally, Fig. 9(c) shows the diagonal elements of the QD density matrix for the ground singlet state $|n_{\rm ref}+1, 0\rangle$. P_n is the probability that the QD is in a state with occupation n. A crossover from a large magnetic moment in the Kondo regime (large P_1) toward ABSs (large $P_0 + P_2$) is evident.

To obtain experimentally relevant results, from this point on we set U to a value appropriate for contemporary InAs nanowire QD devices with top gates [41], $U/\Delta = 4$. The vertical dashed line at $U = 4\Delta$ in all panels of Fig. 9 demonstrates that this situation is far away from either limit, i.e., in the regime where charge fluctuations are important and the singlet states are neither YSR nor ABS. This competition between U, Δ, and E_C thus opens a new degree of complexity in the formation of the eigenstates [31,41]. The subgap states are not simple combinations of singlets that we had previously examined but rather some more complicated entities that generally exhibit noninteger occupation in each system component. The competition reduces the local moment on the QD, which diminishes the importance of hybridization. We demonstrate the effect in Fig. 10, where the Γ_R dependence of the subgap spectra is shown for $U = 4\Delta$. The decreased importance of Γ becomes obvious when one compares this

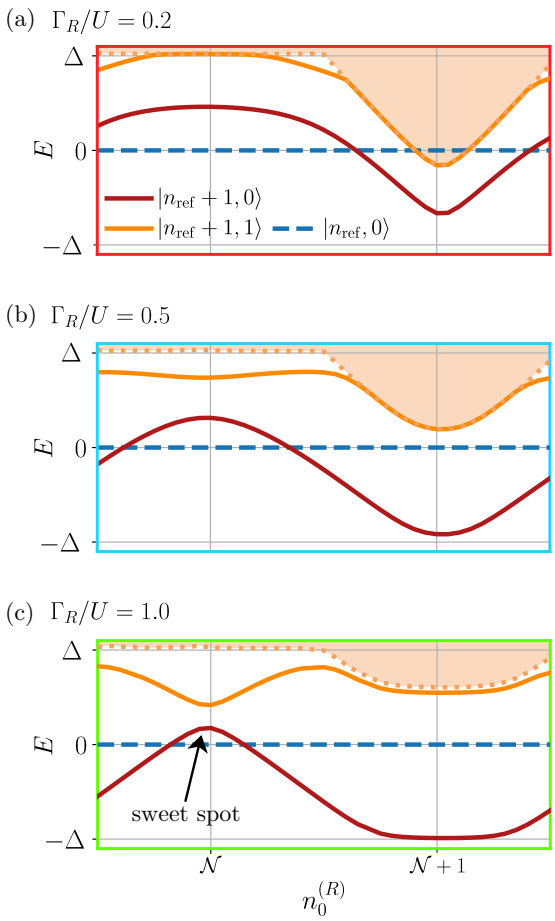

FIG. 11. Subgap spectra with a realistic value of $U = 4\Delta$, $E_C^{(L)} = 0.1\Delta$, and $E_C^{(R)} = 1.5\Delta$. Varying $n_0^{(R)}$ and (top to bottom) increasing Γ_R. The colors of the panel frames correspond to vertical dotted lines in Fig. 10, indicating the position of the cut.

plot to Fig. 7(a), which is equal in all parameters but at much larger U.

VI. GATE VOLTAGE TUNING

In the following section, we investigate the gate voltage dependencies on the SC islands and in the QD. We mainly focus on the regime with two nearby subgap states presented in Sec. IV C, but with $U = 4\Delta$. The goal in this section is twofold. First, we presented results in the experimentally relevant regime. Second, we point out the optimal points for the operation of a proposed YSR qubit and show that they occur when the energy difference between the subgap states has a stationary point, i.e. is minimal.

A. SC island gate voltage tuning

Figure 11 illustrates the transformation of the subgap spectra with varying $n_0^{(R)}$ (the gate voltage setting the occupancy of the right SC island) for a range of Γ_R. By tuning $n_0^{(R)}$ toward an odd integer value $\mathcal{N}+1$, the large $E_C^{(R)}$ enforces odd occupation in the right channel. This results in the decoupling of the left channel in a large interval around odd $n_0^{(R)}$ and a single YSR-like subgap singlet. This is the same decoupling effect

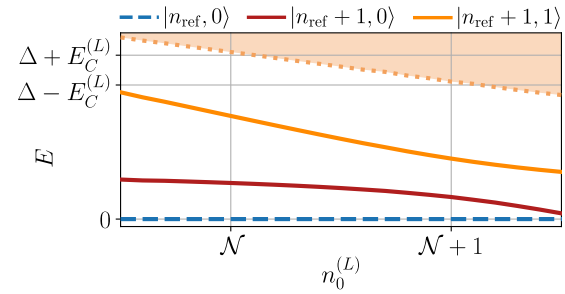

FIG. 12. Subgap spectra with varying $n_0^{(L)}$. Realistic value of $U = 4\Delta$, at the strongly asymmetric point with $E_C^{(L)} = 0.1\Delta$ and $E_C^{(R)} = 1.5\Delta$ and $\Gamma_L/U = 0.1U$, $\Gamma_R/U = 1$. The energy difference between the singlets has a minimum at $n_0^{(L)} \sim \mathcal{N}$.

as seen in Fig. 6, where odd occupation of the right channel is enforced by a large $E_C^{(L)}$ term at even $n_0^{(L)}$. As $E_C^{(R)} > \Delta$, we observe the closure of the transport superconducting gap (the difference between the BCS-like doublet state $|\psi_{\rm ref}\rangle$ and the $n_{\rm ref}+1$ quasicontinuum) around odd $n_0^{(R)}$, as predicted in the single-channel model [31]. Increasing Γ_R summons a second bound state into the gap and increases the interval at which it is present. At very large Γ_R and close to $n_0^{(R)} = \mathcal{N}$, the excited subgap state exhibits a further decrease in energy, as exchange of the additional Cooper pair between the channels becomes favorable. The energy difference between the subgap states is minimal at a value of $n_0^{(R)}$ which is somewhat lower than $\mathcal{N}$. This is due to the fact that we are considering the states in the $n_{\rm ref}+1$ sector. These have an additional particle compared to half filling, thus having lower energy (compared to the reference $|\psi_{\rm ref}\rangle$ state) in the $(n_0^{(L)}, n_0^{(R)}) = (\mathcal{N}, \mathcal{N}-\delta)$ parameter point compared to the $(\mathcal{N}, \mathcal{N}+\delta)$ one, where δ represents a small deviation from the half-filling point. If the states in the $n_{\rm ref}-1$ sector were shown instead, the situation would be symmetrically mirrored over the $n_0^{(R)} = \mathcal{N}$ point, with the minimal energy difference at $n_0^{(R)} = \mathcal{N}+\delta$.

Figure 12 shows the $n_0^{(L)}$ dependence of the energy spectrum, corresponding to the case with large hybridization asymmetry shown in Fig. 11(c). The energy of the decoupled continuum states depends linearly on $n_0^{(L)}$, with the slope given by $E_C^{(L)}$. The gap width is $\Delta + E_C^{(L)}$ when $n_0^{(L)} = \mathcal{N}$ and $\Delta - E_C^{(L)}$ when $n_0^{(L)} = \mathcal{N}+1$. While the energies of the states themselves exhibit a finite slope throughout the $n_0^{(L)}$ range, the derivative of the energy *difference* becomes zero close to $n_0^{(L)} = \mathcal{N}+1$. The system thus has an operational sweet spot in both island gate voltage tunings.

B. QD gate voltage tuning

In typical experimental setups, the QD gate voltage is easily tunable as well. In our model, this is represented by the term $U/2(\hat{n}_{\rm imp} - \nu)^2$, where $U/2$ plays the role of the QD charging energy and ν is the favorable occupation of the QD set by the gate. Here we investigate the properties of the spectra for the system in the symmetrical and strongly asymmetrical cases. Tuning the QD gate voltage away from the particle-hole (p-h) symmetric point $\nu = 1$ decreases the local magnetic moment of the dot. A completely filled (or empty) QD thus does not have a local magnetic moment, suppressing

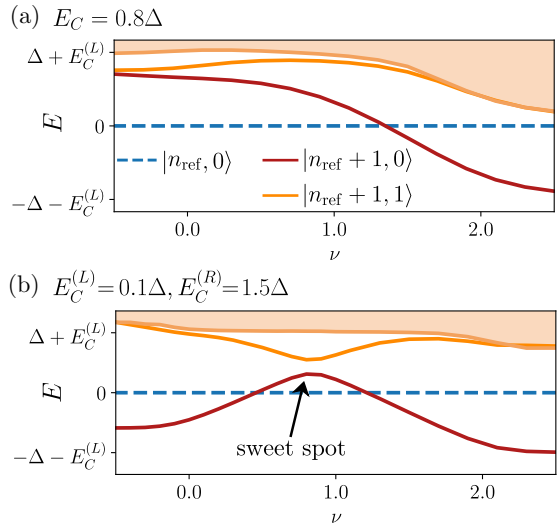

FIG. 13. QD gate voltage tuning with a realistic value of $U \approx 4\Delta$. (a) $E_C^{(L)} = E_C^{(R)} = 0.8\Delta$, $\Gamma_L = \Gamma_R = 0.2U$, (b) $E_C^{(L)} = 0.1\Delta$, $E_C^{(R)} = 1.5\Delta$, $\Gamma_L = 0.1U$, $\Gamma_R = 1.0U$. In both panels, $U = 0.64 = 4\Delta$.

the spin physics entirely. This means that the subgap states asymptotically approach the gap edge for extreme values of ν, resulting in the well-known eye-shaped dispersion for the YSR subgap states.

1. Symmetric case

First we revisit the symmetrical system with $\Gamma_L = \Gamma_R$, $E_C^{(L)} = E_C^{(R)}$, and $n_0^{(L)} = n_0^{(R)} = \mathcal{N}$. We show the energy diagram as a function of ν in Fig. 13(a). In the p-h symmetric point at $\nu = 1$, the singlet subgap states are $|\psi_g\rangle$ and $|\psi_u\rangle$. Deviation from the p-h symmetric point does not break space-inversion symmetry, so the states retain their parity throughout. While increasing ν toward $\nu = 2$, the QD levels fills up, transforming the first subgap state into a $(\mathcal{N}, 2, \mathcal{N})$ configuration. The roles of the singlet and doublet sectors switch, as now the singlet states can be formed without mustering the Bogoliubov quasiparticles, while the doublet states are forced to have odd occupation in the SC islands. The GS in the doublet $n_{\rm ref}$ sector has a full QD level, which is required by $\nu = 2$ and enforced by U. The resulting odd occupation in one of the SC islands results in the energy of this state at $\Delta + E_C$ above the lowest lying singlet state. In the singlet sector, the first excitation consists of a broken Cooper pair in one of the channels, which does not change the occupation of the channels and therefore costs 2Δ. Decreasing ν has the opposite effect of emptying the QD level. The subgap states in the singlet $n_{\rm ref} + 1$ sector are superpositions of the strongly coupled singlet states and states with an empty QD and an additional Cooper pair in the SC: $a(|(\mathcal{N}+2, 0, \mathcal{N})\rangle \pm |(\mathcal{N}, 0, \mathcal{N}+2)\rangle) + b(|\phi_L\rangle \pm |\phi_R\rangle)$, where the plus sign applies to the first (gerade) and the minus sign is for the second (ungerade) subgap state. With decreasing ν, the amplitude a continuously increases at the cost of b as the YSR singlets become less energetically favorable. Despite this, both states remain in the gap throughout the ν range, keeping their gerade/ungerade nature. It should be noted that when $\nu = 0$, the true GS is actually the singlet state in the $n_{\rm ref} - 1$ sector, its energy being equal to that of the $n_{\rm ref} + 1$ GS at $\nu = 2$. The procedure of tuning the device to this point would therefore require two steps: First, tuning the device into the GS at $\nu = 2$ would fill it with $n_{\rm ref} + 1$ electrons. Next, one should completely pinch off the device from the source and drain electrodes by strongly raising the tunnel barriers and, finally, tune the QD gate voltage to $\nu = 0$. The pair of singlet subgap states could then be probed by microwave spectroscopy [65–68].

2. Nonsymmetric case

Next, consider the asymmetrical situation with $E_C^{(L)} \ll E_C^{(R)}$ and $\Gamma_L \ll \Gamma_R$. The energy diagram is shown in Fig. 13(b). The charging energy of the QD and the right channel are comparable and much larger than the charging energy of the left channel. The energy cost of the unfavorable occupation of the left channel is the relatively small factor of $E_C^{(L)}$. Thus the left channel tends to act as a reservoir for the rest of the system, primarily optimizing the charge configuration of the QD and the right channel. The subgap states have $(\mathcal{N}, 1, \mathcal{N}+1)$ and $(\mathcal{N}+2, 1, \mathcal{N}-1)$ configurations at $\nu = 1$. By tuning the gate voltage away from the particle-hole symmetric point, the first subgap state assumes the $(\mathcal{N}+2, 0, \mathcal{N})$ configuration for $\nu = 0$ and $(\mathcal{N}, 2, \mathcal{N})$ for $\nu = 2$. Such configurations do not allow for a second subgap state, as there is no local moment on the QD. The first excitation is a broken Cooper pair in the SC—there is a continuum of such excitations 2Δ above the GS. The value of ν where the energy difference between the two subgap states is minimal is again a bit below half -filling, for the same reasons as when tuning $n_0^{(R)}$.

This is an optimal operation point for a YSR qubit, pointed to by black arrows. The derivative of energy difference with respect to all gate voltages has a root at this triple sweet-spot point, making the system relatively insensitive to electric noise, while the energy difference between the two subgap states itself is minimal. For further comments on the use of the system as a qubit, refer to the Discussion section.

C. Capacitive coupling

Capacitive coupling between component parts of the system is typically present in experimental devices, including in InAs QDs [41,69,70]. We include it in our model by augmenting it with terms that couple charge in parts of the system,

$$V_\beta(\hat{n}_{\rm imp} - \nu)\big(\hat{n}_{\rm SC}^{(\beta)} - \hat{n}_0^{(\beta)}\big), \tag{6}$$

for $\beta = \mathrm{L}, \mathrm{R}$. The strength of the coupling V_β is bounded from above by $\max(U/2, E_C^{(\beta)})$, otherwise the system enters a charge-ordered state [70]. An experimentally relevant value is on the order of $E_C^{(\beta)}/5$ [41]. We find that as long as the ratio of $V_\beta/E_C^{(\beta)}$ is equal for both channels and within reasonable strength, the effect of capacitive coupling on the nature of the subgap singlet states is minute, especially in the proposed qubit regime.

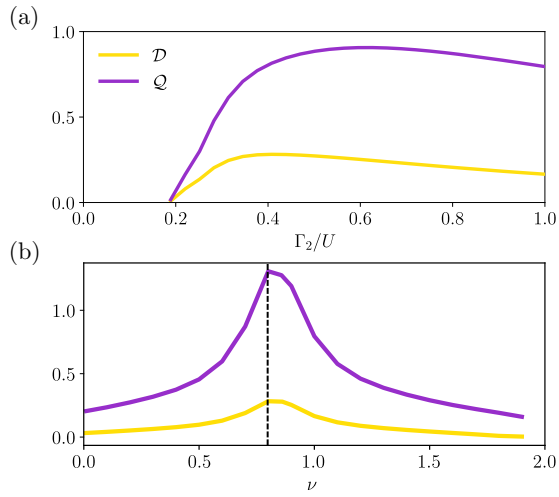

FIG. 14. Electric transition dipole moment $\mathcal{D}$ and quadrupole moment $\mathcal{Q}$. (a) hybridization strength Γ_R dependence for parameters as in Fig. 11(a). (b) QD gate voltage dependence for parameters as in Fig. 13(b). The horizontal dashed line corresponds to the position of the sweet spot in Fig. 13(b).

VII. ELECTRIC TRANSITION MOMENTS

Manipulation of the subgap states in the same charge sector in the SC-QD-SC devices is possible by inducing microwave transitions [71]. The electric field of a linear resonator typically couples to the electric dipole moment of the device [72,73], but coupling to the quadrupole moment is also possible in a triple QD architecture [74]. To demonstrate that manipulation of subgap states in the proposed device is possible, we calculate both quantities for the transitions between the two subgap single states.

The matrix element for the transition dipole moment is $\langle 1|q\hat{\mathbf{r}}|0\rangle$, where $\hat{\mathbf{r}}$ is the position operator. In the language of our model with two pointlike SC islands at unit distance from the QD, this is (up to a constant prefactor) equivalent to $\langle 1|(\hat{n}_L - n_0^{(L)}) - (\hat{n}_R - n_0^{(R)})|0\rangle$. The n_0 factors represent the charge accumulated on the gate electrodes, but their contribution is nullified by the orthogonality of the subgap states. This gives the expression for the transition dipole moment $\mathcal{D} = \langle 1|\hat{n}_L - \hat{n}_R|0\rangle$. Following the same arguments, the quadrupole moment $\langle 1|q\hat{\mathbf{r}}^2|0\rangle$ is written as $\mathcal{Q} = \langle 1|\hat{n}_L + \hat{n}_R|0\rangle$. In Fig. 14, the transition dipole and quadrupole moments for singlet subgap states are shown. Figure 14(a) corresponds to states shown in Fig. 11(a), while Fig. 11(b) corresponds to Fig. 13(b). Both transition moments roughly follow the energy difference between the two singlet states, exhibiting a peak when the singlets are close in energy and the system is close to its sweet spot. Both quickly decrease to zero when one of the states merges with the continuum.

VIII. DISCUSSION

Practical quantum computing, especially one that would be cryptographically relevant, requires systems with a large number of qubits [75]. This need will drive increasing integration and scaling down of all constituent parts. Miniaturization of devices based on superconducting regions will ultimately lead to the use of SC islands, which will then become a ubiquitous element. It thus appears pertinent to explore the possible advantages that these will bring. In this paper, we have studied one possible implementation that makes use of two separate SC islands that bring about two separate spin-singlet YSR subgap states which may be used to store one qubit of information. We now comment on the relation of this class of qubits to other known architectures [76,77] and on its relative merits and downsides.

The YSR spin-singlet qubit may at first appear related to the Andreev qubit in a Josephson junction [78,79]. The Andreev qubit makes use of the ABSs in the even parity subsector: the basis states consist of zero or double occupancy of the ABS. This concept does not directly apply to the YSR spin-singlet states: these cannot be doubly occupied since only a single quasiparticle from a given SC island can bind antiferromagnetically to the impurity to form a singlet state. An Andreev qubit can be approximately modeled using a noninteracting QD which correspond to the $U \to 0$ limit of our model. The higher-energy singlet subgap state of the Andreev qubit at $U \to 0$ is not connected to the higher-energy singlet YSR state at $U \gg \Delta$. Starting from the $U = 0, E_c = 0$ limit, increasing U or E_C will rapidly drive the higher-energy spin-singlet Andreev state into the continuum. Conversely, the higher-energy YSR singlet will disappear in the continuum when moving away from the $U \gg \Delta$, $E_c \neq 0$ regime by decreasing U or E_c.

The YSR singlet qubit is actually more closely related to the charge qubit in double QD systems [80]. The basis states for the charge qubit correspond to the position of the single electron in either of the two QDs. This is similar to YSR singlet qubit states which likewise have different distributions of the wave function in space. In this sense, the SI-QD-SI device is a variant of a charge qubit in a nonhomogeneous triple QD system, however, with the qubit state encoded in a pair of complex many-body states rather than in a single-particle position basis. Depending on the operating point of the device (parameter choice), the spatial structure of the YSR singlets differs. For example, the regime $E_C^{(L)} < E_C^{(R)}$ and $\Gamma_L < \Gamma_R$, discussed in Sec. IV C, corresponds to a pair of singlet states which mainly *differ in the position in space of a single Cooper pair*. In this respect, at this operating point the YSR qubit is actually very similar to the Cooper-pair box charge qubit [81–84].

The YSR singlet qubits are relatively insensitive to magnetic field noise and do not require any magnetic flux tuning through superconducting loops and are in this aspect similar to spin singlet qubits [85,86]. The robustness with respect to magnetic field weakly depends on the g factors of the subsystems (QD versus SC islands). The Zeeman shifts of spin-singlet states are, namely, proportional to the differences in the g factors. Nevertheless, even in the case of different g factors there exist operating points (such as the one discussed above) which are largely insensitive to the field because both states are Zeeman shifted in the same way, since they differ mostly in the position of a Cooper pair (two-particle singlet confined within a single SC island, insensitive to the magnetic field to first order).

Finally, we mention the YSR qubits recently proposed in Ref. [87]. Those are based on classical magnetic moments

(e.g., on high-spin magnetic adsorbates with large magnetic anisotropy) which have spontaneously broken spin symmetry and are sensitive to external magnetic field. Another key difference is that our platform requires a single local moment (QD) and two SCs (SC islands), while their proposal requires two local moments (adatoms) and a singlet SC (surface of a bulk SC). Beside making use of YSR subgap states, the two approaches are thus quite different.

IX. CONCLUSION

We have explored the properties of the subgap states in the system of an interacting QD coupled to two small superconducting islands, focusing on the spin-singlet subspace. We have uncovered regimes where two sub-gap singlets are present deep in the gap with good separation from the continuum states. The two states can never be degenerate, but their energies can be tuned to obtain an energy difference suitable for manipulation with microwaves pulses. The transitions are facilitated by large electric dipole (and quadrupole) transition moments. Such devices could be built using present-day technology. Using a third superconducting island, the scheme could be generalized to qutrits.

This class of devices also has interesting properties in the spin-doublet subspace: two Bogoliubov quasiparticles, one from each superconducting island, could overscreen the impurity moment to produce an overscreened YSR state, a state clearly distinct from the decoupled spin-doublet state.

ACKNOWLEDGMENTS

R.Ž. and L.P. acknowledge the support of the Slovenian Research Agency (ARRS) under No. J1-3008, No. P1-0416, and No. P1-0044. We acknowledge discussions with Daniel Bauernfeind who participated in the early stages of this project. Calculations were performed with the ITensor library [88].

APPENDIX A: TRANSFORMATION TO MIRROR-SYMMETRY-ADAPTED (GERADE/UNGERADE) BASIS

1. Transformation of the BCS Hamiltonian

The mirror-symmetric problem of a QD described by the single-impurity Anderson model that is coupled to two BCS SCs with the same gap Δ and the same superconducting phase ϕ maps to a single-channel problem using a simple transformation to the mirror-symmetry basis (gerade and ungerade parity):

$$g^\dagger_{i,\sigma} = \frac{1}{\sqrt{2}}(c^\dagger_{i,\sigma,L} + c^\dagger_{i,\sigma,R}),$$
$$u^\dagger_{i,\sigma} = \frac{1}{\sqrt{2}}(c^\dagger_{i,\sigma,L} - c^\dagger_{i,\sigma,R}). \tag{A1}$$

One finds

$$\Delta c^\dagger_{i,\uparrow,L} c^\dagger_{i,\downarrow,L} + \Delta c^\dagger_{i,\uparrow,R} c^\dagger_{i,\downarrow,R} + \text{H.c.}$$
$$= \Delta g^\dagger_{i,\uparrow} g^\dagger_{i,\downarrow} + \Delta u^\dagger_{i,\uparrow} u^\dagger_{i,\downarrow} + \text{H.c.} \tag{A2}$$

There are no terms mixing the g/u SC modes, thus the ungerade SC fully decouples from the problem, resulting in a single-channel problem, as is the case for normal-state contacts [89]. At mathematical level this is trivial, but physically it is less so. The cancellation of the mixed gerade/ungerade terms is due to the mean-field decoupling of the effective electron-electron interaction terms and implies the assumption of complete coherence between the condensates in both SC contacts.

If there exists a flux bias ϕ, one proceeds in two steps. First one performs a gauge transformation

$$\tilde{c}^\dagger_{i,\sigma,L} = e^{i\phi/4} c^\dagger_{i,\sigma,L},$$
$$\tilde{c}^\dagger_{i,\sigma,R} = e^{-i\phi/4} c^\dagger_{i,\sigma,R}, \tag{A3}$$
$$\tilde{d}^\dagger_{\sigma} = e^{i\phi/4} d^\dagger_{\sigma}.$$

One then performs a transformation to g/u basis in terms of $\tilde{c}$ operators:

$$g^\dagger_{i,\sigma} = \frac{1}{\sqrt{2}}(\tilde{c}^\dagger_{i,\sigma,L} + \tilde{c}^\dagger_{i,\sigma,R}),$$
$$u^\dagger_{i,\sigma} = \frac{1}{\sqrt{2}}(\tilde{c}^\dagger_{i,\sigma,L} - \tilde{c}^\dagger_{i,\sigma,R}). \tag{A4}$$

One finds

$$\Delta e^{i\phi/2} c^\dagger_{i,\uparrow,L} c^\dagger_{i,\downarrow,L} + \Delta e^{-i\phi/2} c^\dagger_{i,\uparrow,R} c^\dagger_{i,\downarrow,R} + t\sum_\sigma c^\dagger_{i,\sigma,L} d_\sigma + t\sum_\sigma c^\dagger_{i,\sigma,R} d_\sigma + \text{H.c.}$$
$$= \Delta g^\dagger_{i,\uparrow} g^\dagger_{i,\downarrow} + \Delta u^\dagger_{i,\uparrow} u^\dagger_{i,\downarrow} + \sqrt{2}t\cos(\phi/4)\sum_\sigma g^\dagger_{i,\sigma} d_\sigma + i\sqrt{2}t\sin(\phi/4)\sum_\sigma u^\dagger_{i,\sigma} d_\sigma + \text{H.c.} \tag{A5}$$

The QD is coupled to the g modes with the hybridization multiplied by a factor $2\cos^2(\phi/4)$ and to the u modes with a factor $2\sin^2(\phi/4)$ [90]. In the presence of phase bias, the u modes thus do not decouple. This leads to the second singlet YSR state [63].

More generally, for an Anderson-model QD coupled to an arbitrary number of BCS SCs with arbitrary hybridization strengths and arbitrary gap parameters (amplitude and phase), the BCS SCs can be integrated out, resulting in a single hybridization function in the Nambu space. In this sense, the problem is always effectively a single-channel problem.

Nevertheless, the nontrivial structure of the hybridization matrix as a function of frequency reflects the complexity of the setup and can lead to, for example, the existence of multiple singlet YSR states in the presence of flux biases.

2. Transformation of the Richardson model

Given that the Richardson model is equivalent to the BCS model in the limit of large N, a similar procedure is possible. Applying the even odd transformation Eq. (A1) to the number-conserving pairing Hamiltonian,

$$\sum_{i,j}^{N} c^{\dagger}_{i,\uparrow,L} c^{\dagger}_{i,\downarrow,L} c_{j,\downarrow,L} c_{j,\uparrow,L} + \sum_{i,j}^{N} c^{\dagger}_{i,\uparrow,R} c^{\dagger}_{i,\downarrow,R} c_{j,\downarrow,R} c_{j,\uparrow,R}, \quad \text{(A6)}$$

one finds three types of terms. There are intrachannel pairing terms,

$$u^{\dagger}_{i,\uparrow} u^{\dagger}_{i,\downarrow} u_{j,\downarrow} u_{j,\uparrow} + g^{\dagger}_{j,\uparrow} g^{\dagger}_{j,\downarrow} g_{i,\downarrow} g_{i,\uparrow}, \quad \text{(A7)}$$

the terms that pair levels between channels,

$$u^{\dagger}_{i,\uparrow} u^{\dagger}_{i,\downarrow} g_{j,\downarrow} g_{j,\uparrow} + g^{\dagger}_{j,\uparrow} g^{\dagger}_{j,\downarrow} u_{i,\downarrow} u_{i,\uparrow}, \quad \text{(A8)}$$

and, finally, the terms that mix single-particle states from both channels:

$$u^{\dagger}_{i,\uparrow} g^{\dagger}_{i,\downarrow} u_{j,\downarrow} g_{j,\uparrow} + g^{\dagger}_{j,\uparrow} u^{\dagger}_{j,\downarrow} g_{i,\downarrow} u_{i,\uparrow}, \quad \text{(A9)}$$

$$u^{\dagger}_{i,\uparrow} g^{\dagger}_{i,\downarrow} g_{j,\downarrow} u_{j,\uparrow} + g^{\dagger}_{j,\uparrow} u^{\dagger}_{j,\downarrow} u_{i,\downarrow} g_{i,\uparrow}. \quad \text{(A10)}$$

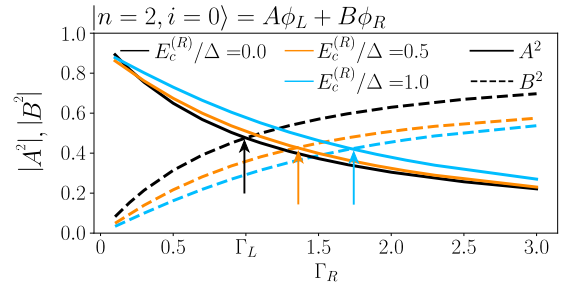

FIG. 15. Probabilities of the $|\phi_L\rangle$ and $|\phi_R\rangle$ states for the lowest lying singlet state in the zero-bandwidth approximation ($\mathcal{N} = 1$). The colored arrows point to the $|A^2| = |B^2|$ points. $E_C^{(L)} = 0$, various $E_C^{(R)}$. $N = 1, U = 10, \Gamma_L = 1$.

The terms which couple u and g modes have a random phase and give zero contribution in the limit of $N \to \infty$. The two channels therefore decouple in the Richardson model too.

APPENDIX B: MPO REPRESENTATION

Here we provide the MPO representation of the Hamiltonian studied in this paper. It is implemented with the impurity in the middle of the system, with N sites on each side of it. An alternative implementation is possible with the impurity as the leftmost site. We obtain exactly the same results with both approaches and do not observe very significant differences in the computational efficiency between the two implementations. Leftmost site (1 denotes the first level in the left channel):

$$W_1 = I\big(\big[\epsilon_1 + E_C^{(L)}\big(1-2n_0^{(L)}\big)\big]\hat{n}_1 + \big(g + 2E_C^{(L)}\big)\hat{n}_{1\uparrow}\hat{n}_{1\downarrow}\; vc^{\dagger}_{1\uparrow}F_1\; vc^{\dagger}_{1\downarrow}F_1\; - vc_{1\uparrow}F_1\; - vc_{1\downarrow}F_1\; gc_{1\downarrow}c_{1\uparrow}\; gc^{\dagger}_{1\uparrow}c^{\dagger}_{1\downarrow}\; 2E_C^{(L)}n_1\big). \quad \text{(B1)}$$

Here $F_i = (-1)^n$ is the local fermionic-parity operator, which gives a phase of -1 if there is an odd number of electrons on the site. Charge operators are

$$\hat{n}_{i\sigma} = c^{\dagger}_{i\sigma} c_{i\sigma}, \quad \hat{n}_i = \sum_{\sigma} \hat{n}_{i\sigma}. \quad \text{(B2)}$$

Generic site in the left half of the system (i denotes a level in the left channel):

$$W_i = \begin{pmatrix} 1 & \big[\epsilon_i + E_C^{(L)}\big(1-2n_0^{(L)}\big)\big]\hat{n}_i + (g+2E_C^{(L)})\hat{n}_{i\uparrow}\hat{n}_{i\downarrow} & vc^{\dagger}_{i\uparrow}F_i & vc^{\dagger}_{i\downarrow}F_i & -vc_{i\uparrow}F_i & -vc_{i\downarrow}F_i & gc_{i\downarrow}c_{i\uparrow} & gc^{\dagger}_{i\uparrow}c^{\dagger}_{i\downarrow} & 2E_C^{(L)}\hat{n}_i \\ 0 & I & 0 & 0 & 0 & 0 & 0 & 0 & 0 \\ 0 & 0 & F_i & 0 & 0 & 0 & 0 & 0 & 0 \\ 0 & 0 & 0 & F_i & 0 & 0 & 0 & 0 & 0 \\ 0 & 0 & 0 & 0 & F_i & 0 & 0 & 0 & 0 \\ 0 & 0 & 0 & 0 & 0 & F_i & 0 & 0 & 0 \\ 0 & c^{\dagger}_{i\uparrow}c^{\dagger}_{i\downarrow} & 0 & 0 & 0 & 0 & I & 0 & 0 \\ 0 & c_{i\downarrow}c_{i\uparrow} & 0 & 0 & 0 & 0 & 0 & I & 0 \\ 0 & \hat{n}_i & 0 & 0 & 0 & 0 & 0 & 0 & I \end{pmatrix}. \quad \text{(B3)}$$

Impurity site:

$$W_{\text{imp}} = \begin{pmatrix} 1 & \epsilon_{\text{imp}}\hat{n}_{\text{imp}} + U\hat{n}_{\text{imp}\uparrow}\hat{n}_{\text{imp}\downarrow} & -d^{\dagger}_{\uparrow}F & -d^{\dagger}_{\downarrow}F & d_{\uparrow}F & d_{\downarrow}F & 0 & 0 & 0 \\ 0 & I & 0 & 0 & 0 & 0 & 0 & 0 & 0 \\ 0 & d_{\uparrow} & 0 & 0 & 0 & 0 & 0 & 0 & 0 \\ 0 & d_{\downarrow} & 0 & 0 & 0 & 0 & 0 & 0 & 0 \\ 0 & d^{\dagger}_{\uparrow} & 0 & 0 & 0 & 0 & 0 & 0 & 0 \\ 0 & d^{\dagger}_{\downarrow} & 0 & 0 & 0 & 0 & 0 & 0 & 0 \\ 0 & 0 & 0 & 0 & 0 & 0 & 0 & 0 & 0 \\ 0 & 0 & 0 & 0 & 0 & 0 & 0 & 0 & 0 \\ 0 & 0 & 0 & 0 & 0 & 0 & 0 & 0 & 0 \end{pmatrix}. \quad \text{(B4)}$$

Generic site in the right half of the system (i denotes a level in the right channel):

$$W_i = \begin{pmatrix} 1 & \left[\epsilon_i + E_C^{(R)}\left(1-2n_0^{(R)}\right)\right]\hat{n}_i + \left(g+2E_C^{(R)}\right)\hat{n}_{i\uparrow}\hat{n}_{i\downarrow} & 0 & 0 & 0 & 0 & gc_{i\downarrow}c_{i\uparrow} & gc_{i\uparrow}^\dagger c_{i\downarrow}^\dagger & 2E_C^{(R)}\hat{n}_i \\ 0 & I & 0 & 0 & 0 & 0 & 0 & 0 & 0 \\ 0 & vc_{i\uparrow}^\dagger & F_i & 0 & 0 & 0 & 0 & 0 & 0 \\ 0 & vc_{i\downarrow}^\dagger & 0 & F_i & 0 & 0 & 0 & 0 & 0 \\ 0 & vc_{i\uparrow} & 0 & 0 & F_i & 0 & 0 & 0 & 0 \\ 0 & vc_{i\downarrow} & 0 & 0 & 0 & F_i & 0 & 0 & 0 \\ 0 & c_{i\uparrow}^\dagger c_{i\downarrow}^\dagger & 0 & 0 & 0 & 0 & I & 0 & 0 \\ 0 & c_{i\downarrow}c_{i\uparrow} & 0 & 0 & 0 & 0 & 0 & I & 0 \\ 0 & \hat{n}_i & 0 & 0 & 0 & 0 & 0 & 0 & I \end{pmatrix}. \tag{B5}$$

Rightmost site (N denotes the last level in the right channel):

$$W_N = \begin{pmatrix} \left[\epsilon_N + E_C^{(R)}\left(1-2n_0^{(R)}\right)\right]\hat{n}_N + \left(g+2E_C^{(R)}\right)\hat{n}_{N\uparrow}\hat{n}_{N\downarrow} \\ I \\ vc_{N\uparrow}^\dagger \\ vc_{N\downarrow}^\dagger \\ vc_{N\uparrow} \\ vc_{N\downarrow} \\ c_{N\uparrow}^\dagger c_{N\downarrow}^\dagger \\ c_{N\downarrow}c_{N\uparrow} \\ \hat{n}_N \end{pmatrix}. \tag{B6}$$

APPENDIX C: ZERO-BANDWIDTH CALCULATION OF CHANGING NATURE OF SUBGAP STATES

The contribution of the left and right channel singlets can be directly calculated in the zero bandwidth limit (the SC islands are represented by a single level, $N = 1$), where the singlet GS with two particles is $|n = 2, i = 0\rangle \approx A|\phi_L\rangle + B|\phi_R\rangle$. Figure 15 shows the Γ_R dependence of the probability amplitudes A and B. Colored arrows point to the $|A| = |B|$ points, where the state is an equal superposition of the left and right channel singlets. When $E_C^{(L)} = E_C^{(R)} = 0$, the equal superposition point occurs exactly at $\Gamma_L = \Gamma_R$, while it is pushed toward larger Γ_R with increasing $E_C^{(R)}$.

[1] L. Yu, Bound state in superconductors with paramagnetic impurities, Acta Phys. Sin. **21**, 75 (1965).

[2] H. Shiba, Classical spins in superconductors, Prog. Theor. Phys. **40**, 435 (1968).

[3] A. I. Rusinov, Superconductivity near a paramagnetic impurity, Sov. J. Exp. Theor. Phys. Lett. **9**, 85 (1969).

[4] A. V. Balatsky, I. Vekhter, and Jian-Xin Zhu, Impurity-induced states in conventional and unconventional superconductors, Rev. Mod. Phys. **78**, 373 (2006).

[5] A. Martín-Rodero and A. Levy Yeyati, Josephson and Andreev transport through quantum dots, Adv. Phys. **60**, 899 (2011).

[6] B. W. Heinrich, J. I. Pascual, and K. J. Franke, Single magnetic adsorbates on s -wave superconductors, Prog. Surf. Sci. **93**, 1 (2018).

[7] R. M. Lutchyn, E. P. A. M. Bakkers, L. P. Kouwenhoven, P. Krogstrup, C. M. Marcus, and Y. Oreg, Majorana zero modes in superconductor–semiconductor heterostructures, Nat. Rev. Mater. **3**, 52 (2018).

[8] V Meden, The Anderson–Josephson quantum dot—a theory perspective, J. Phys.: Condens. Matter **31**, 163001 (2019).

[9] E. Prada, P. San-Jose, M. W. A. de Moor, A. Geresdi, E. J. H. Lee, J. Klinovaja, D. Loss, J. Nygård, R. Aguado, and L. P. Kouwenhoven, From Andreev to Majorana bound states in hybrid superconductor–semiconductor nanowires, Nat. Rev. Phys. **2**, 575 (2020).

[10] S. M. Frolov, M. J. Manfra, and J. D. Sau, Topological superconductivity in hybrid devices, Nat. Phys. **16**, 718 (2020).

[11] P. W. Anderson, Localized magnetic states in metals, Phys. Rev. **124**, 41 (1961).

[12] J. Bardeen, L. N. Cooper, and J. R. Schrieffer, Microscopic theory of superconductivity, Phys. Rev. **106**, 162 (1957).

[13] K. G. Wilson, The renormalization group: Critical phenomena and the Kondo problem, Rev. Mod. Phys. **47**, 773 (1975).

[14] H. R. Krishna-murthy, J. W. Wilkins, and K. G. Wilson, Renormalization-group approach to the Anderson model of dilute magnetic alloys. II. Static properties for the asymmetric case, Phys. Rev. B **21**, 1044 (1980).

[15] R. Bulla, T. A. Costi, and T. Pruschke, Numerical renormalization group method for quantum impurity systems, Rev. Mod. Phys. **80**, 395 (2008).

[16] O. Sakai, Y. Shimizu, H. Shiba, and K. Satori, Numerical renormalization group study of magnetic impurities in superconductors. II. Dynamical excitation spectra and spatial variation of the order parameter, J. Phys. Soc. Jpn. **62**, 3181 (1993).

[17] T. Yoshioka and Y. Ohashi, Numerical renormalization group studies on single impurity Anderson model in superconductivity: A unified treatment of magnetic, nonmagnetic impurities, and resonance scattering, J. Phys. Soc. Jpn. **69**, 1812 (2000).

[18] K. Satori, H. Shiba, O. Sakai, and Y. Shimizu, Numerical renormalization group study of magnetic impurities in superconductors, J. Phys. Soc. Jpn. **61**, 3239 (1992).

[19] P. Krogstrup, N. L. B. Ziino, W. Chang, S. M. Albrecht, M. H. Madsen, E. Johnson, J. Nygård, C. M. Marcus, and T. S. Jespersen, Epitaxy of semiconductor–superconductor nanowires, Nat. Mater. **14**, 400 (2015).

[20] W. Chang, S. M. Albrecht, T. S. Jespersen, F. Kuemmeth, P. Krogstrup, J. Nygård, and C. M. Marcus, Hard gap in epitaxial semiconductor–superconductor nanowires, Nat. Nanotechnol. **10**, 232 (2015).

[21] K. Flensberg, Capacitance and conductance of mesoscopic systems connected by quantum point contacts, Phys. Rev. B **48**, 11156 (1993).

[22] K. A. Matveev, Coulomb blockade at almost perfect transmission, Phys. Rev. B **51**, 1743 (1995).

[23] J. von Delft and D. C. Ralph, Spectroscopy of discrete energy levels in ultrasmall metallic grains, Phys. Rep. **345**, 61 (2001).

[24] W. G. van der Wiel, S. De Franceschi, J. M. Elzerman, T. Fujisawa, S. Tarucha, and L. P. Kouwenhoven, Electron transport through double quantum dots, Rev. Mod. Phys. **75**, 1 (2002).

[25] Y. Oreg and D. Goldhaber-Gordon, Two-Channel Kondo Effect in a Modified Single Electron Transistor, Phys. Rev. Lett. **90**, 136602 (2003).

[26] F. B. Anders, E. Lebanon, and A. Schiller, Coulomb blockade and non-Fermi-liquid behavior in quantum dots, Phys. Rev. B **70**, 201306(R) (2004).

[27] F. B. Anders, E. Lebanon, and A. Schiller, Coulomb blockade and quantum critical points in quantum dots, Phys. B: Condens. Matter **359-361**, 1381 (2005).

[28] H. Zhang, D. E. Liu, M. Wimmer, and L. P. Kouwenhoven, Next steps of quantum transport in Majorana nanowire devices, Nat. Commun. **10**, 5128 (2019).

[29] A. K. Mitchell, A. Liberman, E. Sela, and I. Affleck, SO(5) Non-Fermi Liquid in a Coulomb Box Device, Phys. Rev. Lett. **126**, 147702 (2021).

[30] K. A. Matveev, Quantum fluctuations of the charge of a metal particle under the Coulomb blockade conditions, Zh. Eksp. Teor. Fiz. **99**, 1598 (1991) [Sov. Phys. JETP **72**, 892 (1991)].

[31] L. Pavešić, D. Bauernfeind, and R. Žitko, Yu-Shiba-Rusinov states in superconducting islands with finite charging energy, Phys. Rev. B **104**, L241409 (2021).

[32] D. C. Ralph, C. T. Black, and M. Tinkham, Spectroscopic Measurements of Discrete Electronic States in Single Metal Particles, Phys. Rev. Lett. **74**, 3241 (1995).

[33] D. C. Ralph, C. T. Black, and M. Tinkham, Gate-Voltage Studies of Discrete Electronic States in Aluminum Nanoparticles, Phys. Rev. Lett. **78**, 4087 (1997).

[34] D. Gobert, U. Schollwöck, and J. von Delft, Josephson effect between superconducting nanograins with discrete energy levels, Eur. Phys. J. B **38**, 501 (2004).

[35] R. W. Richardson, A restricted class of exact eigenstates of the pairing-force Hamiltonian, Phys. Lett. **3**, 277 (1963).

[36] R.W. Richardson and N. Sherman, Exact eigenstates of the pairing-force Hamiltonian, Nucl. Phys. **52**, 221 (1964).

[37] J. von Delft and F. Braun, Superconductivity in ultrasmall grains: Introduction to Richardson's exact solution, arXiv:cond-mat/9911058v1.

[38] U. Schollwöck, The density-matrix renormalization group, Rev. Mod. Phys. **77**, 259 (2005).

[39] S. R. White, Density Matrix Formulation for Quantum Renormalization Groups, Phys. Rev. Lett. **69**, 2863 (1992).

[40] Steven R. White, Density-matrix algorithms for quantum renormalization groups, Phys. Rev. B **48**, 10345 (1993).

[41] J. C. E. Saldaña, A. Vekris, L. Pavešić, P. Krogstrup, R. Žitko, K. Grove-Rasmussen, and J. Nygård, Excitations in a superconducting Coulombic energy gap, arXiv:2101.10794.

[42] S. D. Franceschi, L. Kouwenhoven, C. Schönenberger, and W. Wernsdorfer, Hybrid superconductor–quantum dot devices, Nat. Nanotechnol. **5**, 703 (2010).

[43] R. Aguado, A perspective on semiconductor-based superconducting qubits, Appl. Phys. Lett. **117**, 240501 (2020).

[44] J.-D. Pillet, C. H. L. Quay, P. Morfin, C. Bena, A. Levy Yeyati, and P. Joyez, Andreev bound states in supercurrent-carrying carbon nanotubes revealed, Nat. Phys. **6**, 965 (2010).

[45] W. Chang, V. E. Manucharyan, T. S. Jespersen, J. Nygård, and C. M. Marcus, Tunneling Spectroscopy of Quasiparticle Bound States in a Spinful Josephson Junction, Phys. Rev. Lett. **110**, 217005 (2013).

[46] L. Casparis, T. W. Larsen, M. S. Olsen, F. Kuemmeth, P. Krogstrup, J. Nygård, K. D. Petersson, and C. M. Marcus, Gatemon Benchmarking and Two-Qubit Operations, Phys. Rev. Lett. **116**, 150505 (2016).

[47] L. Casparis, M. R. Connolly, M. Kjaergaard, N. J. Pearson, A. Kringhøj, T. W. Larsen, F. Kuemmeth, T. Wang, C. Thomas, S. Gronin, G. C. Gardner, M. J. Manfra, C. M. Marcus, and K. D. Petersson, Superconducting gatemon qubit based on a proximitized two-dimensional electron gas, Nat. Nanotechnol. **13**, 915 (2018).

[48] P. D. Kurilovich, V. D. Kurilovich, V. Fatemi, M. H. Devoret, and L. I. Glazman, Microwave response of an Andreev bound state, Phys. Rev. B **104**, 174517 (2021).

[49] I. Affleck, Non-fermi liquid behavior in Kondo models, J. Phys. Soc. Jpn. **74**, 59 (2005).

[50] R. M. Potok, I. G. Rau, H. Shtrikman, Y. Oreg, and D. Goldhaber-Gordon, Observation of the two-channel Kondo effect, Nature (London) **446**, 167 (2007).

[51] Z. Iftikhar, S. Jezouin, A. Anthore, U. Gennser, F. D. Parmentier, A. Cavanna, and F. Pierre, Two-channel Kondo effect and renormalization flow with macroscopic quantum charge states, Nature (London) **526**, 233 (2015).

[52] S. Kirchner, Two-channel kondo physics: From engineered structures to quantum materials realizations, Adv. Quantum Technol. **3**, 1900128 (2020).

[53] R. Žitko and M. Fabrizio, Non-Fermi-liquid behavior in quantum impurity models with superconducting channels, Phys. Rev. B **95**, 085121 (2017).

[54] F. Braun and J. von Delft, Fixed-N Superconductivity: The Crossover from the Bulk to the Few-Electron Limit, Phys. Rev. Lett. **81**, 4712 (1998).

[55] F. Braun and J. von Delft, Superconductivity in ultrasmall metallic grains, Phys. Rev. B **59**, 9527 (1999).

[56] D. V. Averin and Yu. V. Nazarov, Single-Electron Charging of a Superconducting Island, Phys. Rev. Lett. **69**, 1993 (1992).

[57] P. Lafarge, P. Joyez, D. Esteve, C. Urbina, and M. H. Devoret, Measurement of the Even-Odd Free-Energy Difference of an Isolated Superconductor, Phys. Rev. Lett. **70**, 994 (1993).

[58] J. von Delft, A. D. Zaikin, D. S. Golubev, and W. Tichy, Parity-Affected Superconductivity in Ultrasmall Metallic Grains, Phys. Rev. Lett. **77**, 3189 (1996).

[59] K. A. Matveev and A. I. Larkin, Parity Effect in Ground State Energies of Ultrasmall Superconducting Grains, Phys. Rev. Lett. **78**, 3749 (1997).

[60] A. Mastellone, G. Falci, and Rosario Fazio, Small Superconducting Grain in the Canonical Ensemble, Phys. Rev. Lett. **80**, 4542 (1998).

[61] M. T. Tuominen, J. M. Hergenrother, T. S. Tighe, and M. Tinkham, Experimental Evidence for Parity-Based 2*e* Periodicity in a Superconducting Single-Electron Tunneling Transistor, Phys. Rev. Lett. **69**, 1997 (1992).

[62] M. Tinkham, *Introduction to Superconductivity*, 2nd ed. (Dover Publications, New York, 2004).

[63] G. Kiršanskas, M. Goldstein, K. Flensberg, L. I. Glazman, and J. Paaske, Yu-Shiba-Rusinov states in phase-biased superconductor–quantum dot–superconductor junctions, Phys. Rev. B **92**, 235422 (2015).

[64] J. R. Schrieffer and P. A. Wolff, Relation between the Anderson and Kondo Hamiltonians, Phys. Rev. **149**, 491 (1966).

[65] G. de Lange, B. van Heck, A. Bruno, D. J. van Woerkom, A. Geresdi, S. R. Plissard, E. P. A. M. Bakkers, A. R. Akhmerov, and L. DiCarlo, Realization of Microwave Quantum Circuits using Hybrid Superconducting-Semiconducting Nanowire Josephson Elements, Phys. Rev. Lett. **115**, 127002 (2015).

[66] T. W. Larsen, K. D. Petersson, F. Kuemmeth, T. S. Jespersen, P. Krogstrup, J. Nygård, and C. M. Marcus, Semiconductor-Nanowire-Based Superconducting Qubit, Phys. Rev. Lett. **115**, 127001 (2015).

[67] D. J. van Woerkom, A. Proutski, B. van Heck, D. Bouman, J. I. Väyrynen, L. I. Glazman, P. Krogstrup, J. Nygård, L. P. Kouwenhoven, and A. Geresdi, Microwave spectroscopy of spinful Andreev bound states in ballistic semiconductor Josephson junctions, Nat. Phys. **13**, 876 (2017).

[68] L. Tosi, C. Metzger, M. F. Goffman, C. Urbina, H. Pothier, S. Park, A. L. Yeyati, J. Nygård, and P. Krogstrup, Spin-Orbit Splitting of Andreev States Revealed by Microwave Spectroscopy, Phys. Rev. X **9**, 011010 (2019).

[69] M. R Galpin, D. E. Logan, and H. R. Krishnamurthy, Renormalization group study of capacitively coupled double quantum dots, J. Phys.: Condens. Matter **18**, 6545 (2006).

[70] Y. Nishikawa, D. J. G. Crow, and A. C. Hewson, Phase diagram and critical points of a double quantum dot, Phys. Rev. B **86**, 125134 (2012).

[71] T. H. Oosterkamp, T. Fujisawa, W. G. van der Wiel, K. Ishibashi, R. V. Hijman, S. Tarucha, and L. P. Kouwenhoven, Microwave spectroscopy of a quantum-dot molecule, Nature (London) **395**, 873 (1998).

[72] A. Wallraff, D. I. Schuster, A. Blais, L. Frunzio, R.-S. Huang, J. Majer, S. Kumar, S. M. Girvin, and R. J. Schoelkopf, Strong coupling of a single photon to a superconducting qubit using circuit quantum electrodynamics, Nature (London) **431**, 162 (2004).

[73] A. Stockklauser, P. Scarlino, J. V. Koski, S. Gasparinetti, C. K. Andersen, C. Reichl, W. Wegscheider, T. Ihn, K. Ensslin, and A. Wallraff, Strong Coupling Cavity QED with Gate-Defined Double Quantum Dots Enabled by a High Impedance Resonator, Phys. Rev. X **7**, 011030 (2017).

[74] J. V. Koski, A. J. Landig, M. Russ, J. C. Abadillo-Uriel, P. Scarlino, B. Kratochwil, C. Reichl, W. Wegscheider, Guido Burkard, Mark Friesen, S. N. Coppersmith, A. Wallraff, K. Ensslin, and T. Ihn, Strong photon coupling to the quadrupole moment of an electron in a solid-state qubit, Nat. Phys. **16**, 642 (2020).

[75] D. Loss and D. P. DiVincenzo, Quantum computation with quantum dots, Phys. Rev. A **57**, 120 (1998).

[76] M. A. Nielsen and I. L. Chuang, *Quantum Computation and Quantum Information: 10th Anniversary Edition* (Cambridge University Press, Cambridge, 2010).

[77] M. Kjaergaard, M. E. Schwartz, J. Braumüller, P. Krantz, J. I.-J. Wang, S. Gustavsson, and W. D. Oliver, Superconducting qubits: Current state of play, Annu. Rev. Condens. Matter Phys. **11**, 369 (2020).

[78] C. Janvier, L. Tosi, L. Bretheau, Ç. Ö. Girit, M. Stern, P. Bertet, P. Joyez, D. Vion, D. Esteve, M. F. Goffman, H. Pothier, and C. Urbina, Coherent manipulation of Andreev states in superconducting atomic contacts, Science **349**, 1199 (2015).

[79] M. Hays, G. de Lange, K. Serniak, D. J. van Woerkom, D. Bouman, P. Krogstrup, J. Nygård, A. Geresdi, and M. H. Devoret, Direct Microwave Measurement of Andreev-Bound-State Dynamics in a Semiconductor-Nanowire Josephson Junction, Phys. Rev. Lett. **121**, 047001 (2018).

[80] J. Gorman, D. G. Hasko, and D. A. Williams, Charge-Qubit Operation of an Isolated Double Quantum Dot, Phys. Rev. Lett. **95**, 090502 (2005).

[81] A. Shnirman, G. Schön, and Z. Hermon, Quantum Manipulations of Small Josephson Junctions, Phys. Rev. Lett. **79**, 2371 (1997).

[82] V. Bouchiat, D. Vion, P. Joyez, D. Esteve, and M. H. Devoret, Quantum coherence with a single Cooper pair, Phys. Scr. **T76**, 165 (1998).

[83] Y. Makhlin, G. Schön, and A. Shnirman, Quantum-state engineering with Josephson-junction devices, Rev. Mod. Phys. **73**, 357 (2001).

[84] J. Koch, T. M. Yu, J. Gambetta, A. A. Houck, D. I. Schuster, J. Majer, A. Blais, M. H. Devoret, S. M. Girvin, and R. J. Schoelkopf, Charge-insensitive qubit design derived from the Cooper pair box, Phys. Rev. A **76**, 042319 (2007).

[85] A. Sala and J. Danon, Exchange-only singlet-only spin qubit, Phys. Rev. B **95**, 241303(R) (2017).

[86] A. Sala, J. H. Qvist, and J. Danon, Highly tunable exchange-only singlet-only qubit in a GaAs triple quantum dot, Phys. Rev. Research **2**, 012062(R) (2020).

[87] A. Mishra, P. Simon, T. Hyart, and M. Trif, A Yu-Shiba-Rusinov qubit, PRX Quantum **2**, 040347 (2021).

[88] M. Fishman, S. R. White, and E. M. Stoudenmire, The ITensor software library for tensor network calculations, arXiv:2007.14822.

[89] M. Pustilnik and L. Glazman, Kondo effect in quantum dots, J. Phys.: Condens. Matter **16**, R513 (2004).

[90] M.-S. Choi, M. Lee, K. Kang, and W. Belzig, Kondo effect and Josephson current through a quantum dot between two superconductors, Phys. Rev. B **70**, 020502(R) (2004).